Design of blue crab chitosan responsive nanoparticles as controlled-release nanocarrier: Physicochemical features, thermal stability and in vitro pH-dependent delivery properties

Marwa Hamdi, Rim Nasri, S.M. Li, Moncef Nasri, Murat Kaya, Hela Kchaou, Chentir Imene, Ola Abdelhedi, Mourad Jridi

Manuscript Details

Manuscript number	IJBIOMAC_2019_6140_R1
Title	Design of blue crab chitosan responsive nanoparticles as controlled-release nanocarrier: Physicochemical features, thermal stability and in vitro pH-dependent delivery properties.
Article type	Research Paper

Abstract

In this study, carotenoproteins (CPs) were encapsulated in blue crab chitosan (CS)-tripolyphosphate (TPP) nanoparticules by ionotropic gelation and CS-protein isolate (PI) complex coacervation. The success of CPs encapsulation was confirmed by FT-IR spectroscopy, TGA and XRD techniques. Particle size and thermal stability of nanoparticules was dependent to the encapsulation methods. Indeed, a regular distribution and spherical shape, with size range of about 300 (ionotropic gelation) – 600 nm (complex coacervation), were observed by SEM analysis. The encapsulation efficiency and loading capacity of CPs were about 74% and 31% for the complex coacervation and 89% and 47% for the ionotropic gelation approaches, respectively. In vitro release studies showed an initial swift effect, followed by a slow CPs release. The highest amount of released CPs and the lowest release time were detected with the ionotropic gelation method. Further, in vitro release kinetics of CPs were found to be medium dependent, where ethanol displayed higher released CPs amount with longer release time, compared to PBS (pH ~ 6.8). These findings suggest that the encapsulation technique obviously affected the particles structure, and the glass transition temperature, and the mass loss of encapsulated materials. The better CPs stabilization was obtained for the ionotropic gelation nanoparticles.

Keywords	Blue crab chitosan; nanoparticles engineering; In vitro release.
Manuscript category	Carbohydrates, Natural Polyacids and Lignins

Corresponding Author	Marwa Hamdi
Corresponding Author's Institution	ENIS
Order of Authors	Marwa Hamdi, Rim Nasri, Suming Li, Moncef Nasri

Suggested reviewers	Murat Kaya, Hela KCHAOU, CHENTIR Imene
Opposed reviewers	Ola Abdelhedi, Mourad Jridi

Submission Files Included in this PDF

File Name [File Type]

Cover Letter R.docx [Cover Letter]

Response Letter IJBM.docx [Response to Reviewers]

Highlights R.docx [Highlights]

Abstract R.docx [Abstract]

Manuscript R.docx [Manuscript File]

Figure captions R.docx [Figure]

Figures R.docx [Figure]

Graphical Abstract R.pdf [Figure]

Tables R.docx [Table]

To view all the submission files, including those not included in the PDF, click on the manuscript title on your EVISE Homepage, then click 'Download zip file'.

Sfax, Tunisia, 26th of September 2019

Dear Editor,

Please find enclosed our revised paper entitled « **Design of blue crab chitosan responsive nanoparticles as controlled-release nanocarrier: Physicochemical features, thermal stability and *in vitro* pH-dependent delivery properties** » to be considered for publication in your journal « **International Journal of Biological Macromolecules** ».

We are in a full awareness of the fact that chitosan use as nanocarrier system is not an innovation in itself, and you may consider our results as have been discussed in the literature or as an expected tenet, but the purpose of our work is, first, the valorization of a species of blue crab that constitutes a real threat to the aquatic Tunisian ecosystem.

Above all of that and concretely, the manuscript discussed the difference between nanoencapsulation techniques, in terms of particles physicochemical features, thermal stability and *in vitro* release kinetics of carotenoproteins, chosen as model.

In this aspect, two approaches were chosen to be investigated, ionotropic gelation and complex coacervation. Regarding the complex coacervation, a new polymer was used, blue crab protein isolate, which was extracted, characterized and applied in our laboratory and it is the subject of another manuscript being submitted.

To this end, several techniques were used to deeply characterize the blue crab chitosan-based nanoparticle, especially, the Scanning Electron and Atomic Force Microscopies, the thermogravimetric and differential scanning calorimetry analyses, etc.

In our opinion, this study would open up a new avenue to understand well the nanoparticles characteristics dependence to the applied technique, helping readers to choose the better nanoencapsulation technique, considering the desired and triggered application.

All authors agree to submit the work to « **International Journal of Biological Macromolecules** ».

This work has not been published before, and is not under consideration for publication anywhere else.

I hope it satisfy the required needs and your approval.

King regard and respect.

Thanking you.

Dr. Marwa HAMDI

Laboratory of Enzymatic Engineering and Microbiology, National School of Engineers of Sfax, Sfax. B.P.1173, 3038 Sfax, Tunisia.

E-mail: marwahamdi50@yahoo.fr

Sfax, Tunisia, September 2019 the 26th

Dear Editor,

We found the reviewers' feedback very helpful. We revised our manuscript and included all their recommendations. These are listed below with our accompanying justifications. We are confident that the clarifications provided here will address all the referees' remarks and we hope that our manuscript will be finally accepted for publication in "Food Hydrocolloids".

Thanking you,

Response to reviewers' comments

Reviewer #1:

First, we thank the reviewer for his constructive and helpful suggestions. All corrections suggested were incorporated in the text and highlighted in red.

This paper untitled «Design of blue crab chitosan responsive nanoparticles as controlled-release nanocarrier: Physicochemical features, thermal stability and *in vitro* pH dependent delivery properties» is well written and structured.

In my opinion the paper presents results which could be published in IJBIOMAC after minor revisions.

In order to improve the quality of the manuscript, the following points should be corrected.

Remarks

1. L 28: replace drug by bioactive molecules;

Yes, we agree with the reviewer comment and mistake corrected as recommended. Please see line 29.

2. L31-34: Please rewrite and be more accurate in the possible avenue of the present work;

Yes, we agree with the reviewer comment and the conclusion in the abstract section was corrected as recommended. Please see lines 32-35.

3. L 49- 50: Such a repetition, please rewrite;

Yes, we agree with the reviewer comment and corrected as recommended.

4. L 49- 50: L 52: Replace “Inactivation” by a more adequate word;

Yes, we agree with the reviewer comment and corrected as recommended.

5. L83 - L83: Please justify the encapsulation of carotenoproteins form blue crab shell with Chitosan and protein isolate from the same blue crab shell;

Yes, we agree with the reviewer and more details were given in the introduction section. Please see lines 77-85:

«*The aim of this study was to encapsulate carotenoproteins from blue crab shells by complex coacervation, using chitosan and protein isolate from the same species, and ionotropic gelation with chitosan and tripolyphosphate. The physicochemical properties, morphology, the pigment storage stability and in vitro release kinetics, were comparatively evaluated, which would open up a new avenue to better understand the nanoparticles characteristics dependence to the applied technique. In fact, blue crab species is, nowadays, extensively found in the Mediterranean, especially, in Tunisian coats causing various damages regarding fishing. Thus, above all of that and concretely, the purpose of our work is additionally the valorization blue crabs used for chitosan, carotenoproteins and protein isolate extraction*».

6. In general, the introduction is unbalanced; there are more details on the encapsulation definitions. it would be interesting to mention some research about chitosane as a nanocarrier, carotenoids encapsulation and its limitation to more highlight the importance of the present study;

Yes, we agree with the reviewer comments and overall the introduction section was improved as recommended.

7. L 91: Why do author mention the phenolic compounds content in CPs?

Authors mention the phenolic compounds content in CPs just to give more details about the chemical composition of CPs, since no further purification steps were conducted. Mistake was corrected. Please see line 91.

8. L 93: Replace recuperation by recovery;

Yes, we agree with the reviewer and the mistake was corrected as recommended. Please see line 91.

9. L113-L114: Repetition;

Yes, we agree with the reviewer and the mistake was corrected as recommended. Please see the Section 2.2.2.

10. L 191 – L193: Justify the chosen temperature and time used in thermal stability;

Yes, we agree with the reviewer and more details were given. Please see lines 203-207:

«*Thermal stability of freeze-dried CS-based nanoparticles based on CS was studied at 80, 100 and 120 °C (sterilization temperatures) for 5, 15 and 30 min, since commercialized products are frequently exposed to heat treatment, the most used processing method in food industry, during their preparation. Particles size and zeta potential were evaluated at each desired time interval*».

11. L213-L225: Too long, please sum up.

In general, the discussion contains too long sentences. It is preferable to shorten the sentences for a better arguments and explanations comprehension.;

Yes, we agree with the overall discussion was revised as recommended.

12. L 327: Delete “in the present work”.

Yes, we agree with the reviewer and the mistake was corrected as recommended. Please see lines 333-334.

13. According the obtained results, the ionotropic gelation was more effective to encapsulate CPs and the obtained nanoparticules could be used in drug delivery. According to the characteristic of CC nanoparticules, which application would author recommend? please add it to the conclusion.;

Yes, we agree with the reviewer and the conclusion was improves as recommended. Please see lines 570-580.

Highlights

- Blue crab chitosan as nanocarrier for carotenoids (CPs) stabilization was used;
- Ionotropic gelation and complex coacervation approaches were adopted;
- Higher entrapment efficiency and loading charge were reached via the ionotropic gelation;
- Microencapsulation enhanced thermal properties and stability of carotenoproteins;
- Ionotropic gelation allowed the highest amount and the lowest release time of CPs.

Abstract

In this study, carotenoproteins (CPs) were encapsulated in blue crab chitosan (CS)-tripolyphosphate (TPP) nanoparticules by ionotropic gelation and CS-protein isolate (PI) complex coacervation. The success of CPs encapsulation was confirmed by FT-IR spectroscopy, TGA and XRD techniques. Particle size and thermal stability of nanoparticules was dependent to the encapsulation methods. Indeed, a regular distribution and spherical shape, with size range of about 300 (ionotropic gelation) – 600 nm (complex coacervation), were observed by SEM analysis. The encapsulation efficiency and loading capacity of CPs were about 74% and 31% for the complex coacervation and 89% and 47% for the ionotropic gelation approaches, respectively. *In vitro* release studies showed an initial swift effect, followed by a slow CPs release. The highest amount of released CPs and the lowest release time were detected with the ionotropic gelation method. Further, *in vitro* release kinetics of CPs were found to be medium dependent, where ethanol displayed higher released CPs amount with longer release time, compared to PBS (pH ~ 6.8). These findings suggest that the encapsulation technique obviously affected the particles structure, and the glass transition temperature, and the mass loss of encapsulated materials. The better CPs stabilization was obtained for the ionotropic gelation nanoparticles.

Keywords: Blue crab chitosan; nanoparticles engineering; *In vitro* release.

Design of blue crab chitosan responsive nanoparticles as controlled-release nanocarrier: Physicochemical features, thermal stability and *in vitro* pH-dependent delivery properties.

Marwa Hamdi [a*], Rim Nasri [a,b], Suming Li [c], Moncef Nasri [a]

[a] Laboratory of Enzyme Engineering and Microbiology, University of Sfax, National Engineering School of Sfax, B.P. 1173, 3038 Sfax, Tunisia.

[b] Higher Institute of Biotechnology of Monastir, University of Monastir, Monastir, Tunisia.

[c] European Institute of Membranes, UMR CNRS 5635, University of Montpellier, Place Eugene Bataillon, 34095 Montpellier Cedex 5, France.

*** Corresponding author:** Marwa Hamdi, Laboratory of Enzyme Engineering and Microbiology, University of Sfax, National Engineering School of Sfax, B.P. 1173, 3038 Sfax, Tunisia. **Tel:** 216 25740373 / 216 54186612; **E-mail:** marwahamdi50@yahoo.fr.

Abstract

In this study, carotenoproteins (CPs) were encapsulated in blue crab chitosan (CS)-tripolyphosphate (TPP) nanoparticules by ionotropic gelation and CS-protein isolate (PI) complex coacervation. The success of CPs encapsulation was confirmed by FT-IR spectroscopy, TGA and XRD techniques. Particle size and thermal stability of nanoparticules was dependent to the encapsulation methods. Indeed, a regular distribution and spherical shape, with size range of about 300 (ionotropic gelation) – 600 nm (complex coacervation), were observed by SEM analysis. The encapsulation efficiency and loading capacity of CPs were about 74% and 31% for the complex coacervation and 89% and 47% for the ionotropic gelation approaches, respectively. *In vitro* release studies showed an initial swift effect, followed by a slow CPs release. The highest amount of released CPs and the lowest release time were detected with the ionotropic gelation method. Further, *in vitro* release kinetics of CPs were found to be medium dependent, where ethanol displayed higher released CPs amount with longer release time, compared to PBS (pH ~ 6.8). These findings suggest that the encapsulation technique obviously affected the particles structure, and the glass transition temperature, and the mass loss of encapsulated materials. The better CPs stabilization was obtained for the ionotropic gelation nanoparticles.

Keywords: Blue crab chitosan; nanoparticles engineering; *In vitro* release.

1. Introduction

Recently, encapsulation has been widely considered as a viable and effective approach for active protection of biomolecules with interesting functional properties. Encapsulation is a process consisting in the incorporation of an active substance into a coating matrix in order to protect it from the external environment (against oxidation and degradation during storage) and control its release in a chosen environment [1,2]. The controlled release process allows encapsulated substances to reach their target in active form [3,4]. Encapsulation has its applications in many areas, including pharmacies for the controlled release of the active ingredient, in cosmetics for the protection of the active ingredient, in food for taste masking, flavor protection, and detergency for encapsulated fragrance for softener or laundry [5].

Various techniques have been developed and used for nanoencapsulation purposes, such as emulsification, coacervation, emulsification–solvent evaporation, nanoprecipitation, supercritical fluid, and inclusion complexation technique. These methods can produce capsules in the nanometer range varying from 10 to 1000 nm [6]. Drug or biomolecules release from nanoparticles takes place by several mechanisms including surface erosion, disintegration, desorption and diffusion [7,8].

A variety of nanoparticles, based on several biocompatible and degradable natural polymers (mainly polysaccharides), has been used. Due to its unique physicochemical and biopharmaceutical properties, in addition to its biodegradable character [9], chitosan is considered effective in drug delivery systems. In fact, in such applications, water solubility and the presence of a positive charge are recommended properties, in order to react with negatively charged polymers, macromolecules and polyanions in an aqueous environment [10]. Thus, chitosan-based delivery systems show great potential for delivering anticancer, antibacterial, antifungal, anti-inflammatory drugs, vaccines, nucleic acids, peptides and therapeutic proteins, DNAs and genes, etc. [11].

Additionally, carotenoids and carotenoproteins are widely applied in food, cosmetics and pharmaceutical industries, because of their various bioactivities, mainly antioxidant, antimicrobial, anticancer, immunomodulatory, antidiabetic and anti-inflammatory effects [12]. Nevertheless, the major difficulties to value their application is their limited solubility/dispersibility in aqueous media and their sensitivity to oxidation and/or degradation, during food processing, drug formulation, etc. [13]. Encapsulation is the emerging technology that offers a mean to overcome these problems, mainly the protection of carotenoids against harsh environmental and the improvement of their stability during processing and storage circumstances [14].

The aim of this study was to encapsulate carotenoproteins from blue crab shells by complex coacervation, using chitosan and protein isolate from the same species, and ionotropic gelation with chitosan and tripolyphosphate. The physicochemical properties, morphology, the pigment storage stability and *in vitro* release kinetics, were comparatively evaluated, which would open up a new avenue to better understand the nanoparticles characteristics dependence to the applied technique. In fact, blue crab species is, nowadays, extensively found in the Mediterranean, especially, in Tunisian coats causing various damages regarding fishing. Thus, above all of that and concretely, the purpose of our work is additionally the valorization blue crabs used for chitosan, carotenoproteins and protein isolate extraction.

2. Materials and methods

2.1. Materials

CS with medium molecular weight of ~125 kDa, acetylation degree of 11% and intrinsic viscosity [η] of 3203 ml/g (0.1% (w/v) in 1% acetic acid) was extracted from blue crab *Portunus segnis* shells, as described in a previous study [15]. CPs, from blue crab shells, contained 4242.86 ± 60.61 μg $g^{-1}_{extract}$ of total carotenoids, with a recovery yield of 84% [16]. Blue crab muscle protein isolate (PI) was prepared based on the pH-shifting method [17], allowing the

recuperation of more than 85% (dry weight) proteins, with an extraction yield of 16% (dry weight).

Tween 80, glacial acetic acid, sodium tripolyphosphate (TPP) and all other chemicals of analytical grade were purchased from Sigma-Aldrich Chemical Co. (St. Louis, USA). Milli-Q water was used throughout this study.

2.2. Conception of blue crab chitosan nanoparticles loaded with carotenoproteins

2.2.1. Encapsulation of CPs into CS-PI nanoparticles by complex coacervation

CS-PI nanoparticles loaded or not with CPs were prepared based on the complex coacervation method by using CS and PI as wall materials, as described by Chang *et al.* [18]. PI at a concentration of 0.5% (w/v) was dissolved in Milli-Q water and solution's pH was adjusted to 10.0 using NaOH 1M, while CS solution (0.5 %, w/v) was prepared in acetic acid 0.15 M (pH 4.0). Both solutions were stirred for 1 h, and then, incubated for 24 h at 4 °C to ensure complete hydration. Afterwards, PI and CS stock solutions were centrifuged at 4 °C, 4000 g for 15 min and supernatants were mixed, to reach the desired PI to CS mass ratios of 1/4, 1/1, 4/1, 8/1, 16/1 and 20/1 (w/w). The mixture was stirred vigorously and stirring was continued for additional 2 h to ensure the cross-linking between CS and PI. In another aspect, complex coacervation pH was optimized considering the zeta potential of aqueous solutions of PI and CS, the turbidity of the PI-CS mixtures and the yield of the dried coacervates measurements [13].

To encapsulate CPs into the nanoparticles, a stock solution was gradually dropped, under vigorously stirring, into the CS stock solution at a CS/CPs mass ratio of 1/0.8. The CPs-loaded nanoparticles were stored at 4 °C overnight to uphold decantation, then, filtered and washed twice with Milli-Q water. To obtain powdered nanoparticles, CS-PI coacervates were lyophilized and stored at 4 °C for subsequent analysis.

The coacervate yield was determined by measuring the coacervate dried mass to the total biopolymer mass in triplicate and expressed as follows [19]:

$$\text{Coacervate yield (\%)} = \frac{M_i}{M_0} \times 100 \qquad \textbf{Eq (1)}$$

where M_0 is the total biopolymers weight used to make the biopolymers solutions and M_i is the weight of the dried coacervate phase.

The PI and CS strength of electrostatic interaction (SEI) at each required pH value was thereby determined. The optimum pH range, which allows complexation to occur between PI and CS, was selected based on the maximum SEI range, and subsequently used to optimize the PI-CS weight ratio.

2.2.2. Encapsulation of CPs in CS-TPP nanoparticles by ionotropic gelation

For the ionotropic gelation, as reported by Haider *et al.* [20], CS solution was prepared, at a concentration of 3.2 mg/ml, in acetic acid 0.15 M. To remove any undissolved particles, CS solution was centrifuged at 3000 g, 4 °C for 15 min. The pH of the solution (50 ml) was adjusted to 4.0. Afterwards, Tween-80 (80 mg) was added as emulsifier and the mixture was stirred at 60 °C for 30 min. Simultaneously, CPs solution was prepared by dissolving 128 mg in 4 ml ethanol, and subsequently gradually dropped, into the CS solution, under vigorously stirring, to reach the desired CS/CPs weight ratio of 1/0.8. Agitation was sustained for 20 min, and then, 30 ml of TPP solution (1.87 mg/ml; pH 4.0) were added drop wise under continuous stirring to the mixture solution for 30 min, to reach a CS-TPP weight ratio of 1/0.35. After complete addition of TPP, mixing was continued for 30 min, to guarantee the complete and the perfect gelation between CS and TPP.

The mixture was, thereafter, centrifuged at 4000 g for 30 min at 4 °C, and the obtained pellet, containing nanoparticles, was rinsed with Milli-Q water (25 ml), and subsequently, freeze-dried.

2.3. Synthetized CPs-loaded CS-based nanoparticles characterizations

2.3.1. Zeta potential and particles size measurement

The zeta potential, as well as the particles size were determined using a laser scattering particles size distribution analyzer Litesizer 500 (Anton Paar, GmbH, France). A minimum of three replicate tests was carried out for each formulation at 25 °C and the mean zeta potential and particles size values, besides standard deviations were obtained with the software included with the instrument.

2.3.2. Turbidimetric analysis

The turbidity was measured with a spectrophotometer (T70, UV/vis spectrometer, PG Instruments Ltd., China) at 600 nm, and the optimum pH for complex coacervation is regarded as the pH value at which the highest light absorption occurred.

2.3.3. CPs encapsulation efficiency and loading charge measurement

The amount of CPs loaded in CS nanoparticles was calculated based on TGA/DTG (derivative thermal gravimetric) analysis [21]. The loading capacity (LC) is defined as the quantity of loaded CPs per 100 g of nanoparticles, while the amount of loaded CPs based on the initial CPs (in feed) corresponds to the encapsulation efficiency (EE). Therefore, considering the DTG thermograms, LC and EE were determined from the equations (2) and (3), respectively, given below:

$$\%\ \mathrm{LC} = \frac{\text{Content of loaded CPs}}{\text{Mass of nanoparticles}} \times 100 \qquad \boldsymbol{Eq\ (2)}$$

$$\%\ \mathrm{EE} = \frac{\text{Content of loaded CPs}}{\text{Content of initial CPs}} \times 100 \qquad \boldsymbol{Eq\ (3)}$$

2.3.4. Spectroscopic characterization of CS nanoparticles

Nanoparticles were applied to the Fourier transform infrared spectroscopy (FTIR, NEXUS of ThermoFisher) equipped with an attenuated reflection accessory (ATR) containing

a diamond/ZnSe crystal, at room temperature (25 °C) in the spectral range frequencies of 650-4000 cm^{-1}. Prior to analysis, calibration was performed via background spectrum recorded from the clean and empty diamond and for each spectrum, 32 scans of interferograms were averaged and the spectral resolution was 4 cm^{-1}. Data analysis and treatment were carried out by using the OMNIC Spectra software (ThermoFisher Scientific).

To further investigate the structural characteristics of the prepared nanoparticles, XRD patterns were recorded using an X-ray diffractometer (D8, Advance Bruker XRD diffractometer, Germany). Ni-filtered Cu Kα radiation (k = 1.5406 ˚A) was used to record the X-ray powder patterns. The relative intensity was recorded in the scattering range 2θ of 5–50° with a step size of 0.02° and a counting time of 5 s/step, with an error of ±1°.

2.3.5. Thermal properties of CS-based nanoparticles

Differential scanning calorimeter (Modulated DSC Q20, TA Instruments), equipped with a liquid nitrogen cooling system, was used to investigate the thermal properties of nanoparticles. The DSC analysis allowed the estimation of melting and crystallization points, as well as the glass transition of the macromolecular materials. Thermal profiles of nanoparticles were analyzed in a temperature range of 0-225 °C, at a heating rate scan of 10 °C/min, under nitrogen flow rate of 50 ml/min. Thermograms were analyzed by using the TA Universal V4.5A software.

Thermal stability of nanoparticles was further studied using Thermogravimetric analyzer (TGA Q500 High Resolution, TA Instruments), operating under nitrogen flow (60 ml/min). TGA analysis is based on the assessment of the progressive change in mass, expressed in percentage (%) as a function of temperature. Samples were heated from 25 to 700 °C at a heating rate of 20 °C/min and their weight, initially about 4 mg, was constantly measured with an accuracy of 0.01 mg. Thermograms were analyzed by using the TA Universal V4.5A software.

2.3.6. Nanoparticles microstructure analysis

The microstructure of nanoparticles was determined using scanning electron microscopy (SEM, Hitachi S4800), at an angle of 90° to the surface, using different magnifications. Prior to imaging, nanoparticles were fixed on the SEM support using double side adhesive tape, and observed up to a 2000 x magnification, under an accelerating voltage of 2.0 kV and an absolute pressure of 60 Pa, after sputter coating with a 5 nm thick gold.

Atomic force microscopy (AFM, Agilent Pico Plus) analysis was performed to further characterize the morphology of unloaded and CPs-loaded CS nanoparticles. Imaging was carried out in tap mode in air with standard Si cantilever, a spring constant of 0.6 N/m and an estimated tip radius of 10 nm. The scan area was 2 µm × 2 µm, 256 lines and taken at a rate of 0.8 s/lines. The study was realized at room temperature with 54% level of humidity. The scan speed was adjusted at 1.01 lines/s, the resonance frequency and the distance between tip and nanoparticles were applied at 161.02 kHz and 9–11 nm, respectively.

2.3.7. Nanoparticles thermal stability

Thermal stability of freeze-dried CS-based nanoparticles based on CS was studied at 80, 100 and 120 °C (sterilization temperatures) for 5, 15 and 30 min, since commercialized products are frequently exposed to heat treatment, the most used processing method in food industry, during their preparation. Particles size and zeta potential were evaluated at each desired time interval.

2.4. Study of CPs *in vitro* release from nanoparticles

Ethanol and PBS (pH ~6.8) were used as media models for an *in vitro* CPs release study. In brief, wet samples (10 mg) and media (1.2 ml) were placed in a microtube and incubated at ambient temperature. At sampling time, the incubated mixture was centrifuged and 100 µl of supernatant was collected. Evaluation of the amount of CPs released was determined using a spectrophotometer at a wavelength of 480 nm. An equal volume of fresh media was then

replaced in the mixture, and the same procedure was repeated for the subsequent sampling. Cumulative percent of released CPs was obtained by dividing the cumulative amount of released CPs at each sampling time point (M_t) to the initial weight of the CPs-loaded in the sample (M_0), and schemed as a function of release time. All *in vitro* release experiments were performed in triplicate.

$$\% \text{ Cumulative release} = \sum_{t=0}^{t} {}^{M_t}\!/_{M_0} \times 100 \qquad \textbf{\textit{Eq}} \ (\mathbf{4})$$

2.5. Statistical analysis

All experiments were carried out in duplicate and average values with standard deviation errors are reported. Mean separation and significance were analyzed using the SPSS software package ver. 17.0 professional edition (SPSS, Inc., Chicago, IL, USA) using ANOVA analysis. Differences were considered significant at $p<0.05$.

3. Results and Discussion

3.1. Optimization of the complex coacervation conditions between CS and PI

3.1.1. Influence of CS and PI solutions' pH

Complex coacervation, the combination of two oppositely-charged polymers causing interaction and precipitation of complex polymers, is a liquid-liquid phase separation mechanism resulting from the formation of intramolecular electrostatic complexes between the macromolecules [22]. In this context, PI and CS complexation was subsequently investigated and optimized.

The evolution of the zeta potential values of the PI and CS solutions in the selected pH range (2.0-10.0) is revealed in **Fig. 1A**. Indeed, the zeta potential of the PI solution was positive below pH 4.5, where negatively charged groups (COO^-) are less abundant than positively charged groups (NH_3^+). For all pH values above pH 4.5, the negativity of the PI increased

gradually with the increase of the pH, where the number of carboxyl groups (COO^-) exceeded the number of amine groups (NH_3^+). The amphoteric character of the proteins containing both amine and carboxyl functional groups resulted in the PI zeta potential pH dependence.

Regarding CS, it was positively charged at pH values below 8.0 and the zeta potential level began to increase with the decrease of pH (**Fig. 1A**). The positive charge of the CS is due to the acid protonation of the amine groups (NH_3^+) of the glucosamine units. The CS zeta potential reduction subsequently to the pH rising could be assigned to the deprotonation of the CS amine groups, by interaction of the proton of the amino group of the CS with strong hydroxyl groups from the added NaOH [18]. This deprotonation led thereby to CS loss of its charge, becoming insoluble at pH values exceeding 8.0.

Since physico-mechanical and thermal characteristics of the complex coacervates are controlled by the extent of the interaction between the contributing matrix-wall polymers, the strength of the electrostatic interaction (SEI), defined as the product of the absolute values of the zeta potential of PI and CS, otherwise, their binding force during complex coacervation, is a critical parameter affecting the complex coacervation process [23]. The SEI values for the PI and CS solutions reached the highest value of approximately 600 mV^2 at pH 6.0, as displayed in **Fig. 1A**, indicating that the strongest attraction between both PI and CS was around this pH value, further supported with an almost neutral zeta potential of PI-CS complex coacervates at pH 6.0.

Additionally, the yield and turbidity of complex coacervates are used as key parameters in the optimization process and are recognized as the most reliable parameters [23]. **Fig. 1B** displays the yield of the complex coacervates at a selected pH range, chosen based on the highest value of SEI (600 mV^2). As it can be seen, the yield of complex coacervates increased significantly ($p<0.05$) with pH increase from pH 4.0 to pH 6.0, suggesting that this range could be the point at which the formation of insoluble complexes was initiated [25]. The highest yield

of 90% ($p<0.05$) was observed at pH 6.0, above which, the yield of complex coacervates started to decrease significantly ($p<0.05$).

This finding was due to an increase of negative charge of PI that was unable to complex with CS (decrease of its positive charge), triggering thereby a disturbance of the charge balance between PI and CS. This optimal pH correlated well with the SEI values that were found to be higher around pH 6.0. Moreover, the decrease in the coacervates yield due to a decrease in the SEI (**Fig. 1A**), and thereby a drop-in complexation between PI and CS, could be due to alkalization of the mixed dispersion above pH of 6.0 leading to dissociation of the complex coacervates.

Turbidity analysis data show similar trend, with a significant ($p<0.05$) decrease in turbidity between pH 6.5 and 8.0, suggesting that the strongest complexation between PI and CS occurred in the pH range of 5.0-6.5, with an optimum at pH 6.0.

3.1.2. PI-to-CS weight balance effect

In another aspect of the complex coacervation optimization, it is recognized that the protein-polysaccharide mixing ratio sensibly influenced the charge balance of their mixture [26]. The turbidity and the coacervate yield of mixtures equilibrium phase, considering different PI to CS mass ratios at an optimal pH of 6.0, are illustrated in **Fig. 1C**. Data reveal that when PI-CS mass ratio increased, the coacervate yield and turbidity values improved significantly ($p<0.05$), reaching the highest levels at the PI-CS ratio of 8/1. An additional increase in PI-CS mass ratios to 20/1 (w/w) resulted in a significant diminution in the coacervates yield and turbidity values ($p<0.05$). In fact, the maximum of coacervate production yield requires the highest quantity of PI and CS moieties in the mixture to be able to interact with each other. However, minor complex coacervate yield could be a consequence of redundant PI-to-CS weight ratios, implying that an outnumber of un-complexed either PI or CS molecules exists [7]. Therefore, the optimal PI-CS mixing ratio of 8/1 was recorded.

3.2. Size and Zeta potential of CPs-loaded nanoparticles

The diameters of CS nanoparticles with and without CPs (ionotropic gelation and complex coacervation) were determined. **Table 1** shows that unloaded nanoparticles obtained by ionotropic gelation and complex coacervation possessed an average diameter of ~7.26 µm and 9.76 µm, and polydispersity indexes of 42.9% and 62.37%, respectively. The mean diameter of CS nanoparticles decreased with the incorporation CPs, with an average diameter of 4.72 µm (ionotropic gelation) and 4.87 µm (complex coacervation) and polydispersity indexes of 37.94% (ionotropic gelation) and 47.04% (complex coacervation), indicating to variable extend the nanoparticles narrow size distribution [3]. The light scattering technique might measure the particle size as reflected by the hydrodynamic diameters of aggregate or hydrated individual particles.

The results reflected that the aqueous aggregation and swelling of CPs-loaded CS nanoparticles were lower than those of unloaded CS nanoparticles, regardless the applied microencapsulation process, i.e. ionotropic gelation or complex coacervation [6]. In fact, the CS nanoparticles are developed based on the electrostatic interaction of CS with TPP (ionotropic gelation) and CS with PI (complex coacervation), which will modulate their size. In another side, the adsorption of CS onto the CPs droplets is the elementary process of CPs-loaded CS nanoparticles formation. The lower agglomeration in CPs-loaded CS nanoparticles might be due to hydrophobic CPs molecules that forced it to entrap inside.

Considering the encapsulation method, different particle sizes distributions were observed for the nanoparticles, being smaller (7.26 to 4.72 µm) for ionotropic gelation than those of the complex coacervation (9.76 to 4.87 µm). This is interesting because the particle size of nanoparticles could sensitively influence their chemical and physical properties [27]. In fact, the smaller particles are more easily solubilized, compared to larger particles with higher surface area. Further, CS molecular weight drop led to the decrease of its viscosity, influencing

the particle size, and the simultaneously increased capability of cross-linking to shape smaller structures [28].

In addition, unloaded nanoparticles exhibited zeta potential values of +51.43 mV and +49.42 mV, for ionotropic gelation and complex coacervation, respectively (**Table 1**). The occurrence of positive zeta potential values, reflecting the specific positively charged surface of CS that could be due to the contribution of protonated amino groups present on the surface of particles [29]. However, the zeta potential decreased to values of +45.3 mV (ionotropic gelation) and +46.8 mV (complex coacervation) for CPs-loaded nanoparticles. This finding reflected that the surface positive charge was reduced due to the loading of CPs and the shielding effect of protonated NH_2 group by CPs on CPs-loaded nanoparticles, mitigating therefore the dispersion stability of nanoparticles in water [30,31]. Although the slight decrease in the zeta potential values after the encapsulation of CPs, the nanoparticules still significantly stable, with zeta potential values exceeding +30 mV [32].

Bagre *et al.* [33] described in a previous work an inversion of positive potential to negative value when alginate was coated over chitosan nanoparticles, with an increase in the size and an improved release profile of enoxaparin facilitating the oral delivery of this bioactive substance. In line with results from the present work, several studies have reported that zeta potential values of CS nanoparticles were reduced when drugs, such as ascorbic acid [34] and eugenol [35] were incorporated.

3.3. Loading charge and entrapment efficiency of CPs

Although spectrophotometry and high-performance liquid chromatography (HPLC) are effective techniques to determine the content of molecules loaded in the particles, these latter were not useful, in the present work. Indeed, CPs did not dissolve in an aqueous HCl solution, besides the complete destruction of particles and dissolution of molecules in the medium that should be considered. Thereby, TGA/DTG thermograms were applied to determine the content

of CPs loaded in nanoparticles [20,36], where CPs-loaded nanoparticles were successfully degraded as described by Wang *et al.* [13].

Fig. 2A shows that CS nanoparticles exhibited three step weight loss at temperatures below 150 °C (moisture loss), 180-310 °C (degradation of CS) and above 310 °C (loss of crosslinked CS with TPP or PI). Compared with the derivative thermogravimetry (DTG) thermograms of the bare nanoparticles, CPs-loaded CS nanoparticles revealed a weight loss in four stages. The new weight loss range, at temperatures ranging from 250 to 310 °C, is ascribed to the degradation of CPs, with a drastic weight mass loss up to 92% in the case of free CPs. The rate of maximum weight loss corresponding to temperature was considered as the decomposition temperature (Td), clearly observed as a peak in the DTG thermogram, as shown in **Fig. 2b**. These results confirmed the successful loading of CPs into CS nanoparticles and the improvement of CPs heat stability by nanoencapsulation, using both systems ionotropic gelation and complex coacervation.

The LC and EE are calculated and presented in **Table 2**, based on the percentage of weight loss at temperatures ranging from 250 to 310 °C, reflecting the amount of loaded CPs, as above described in the section 2.3.3, based on Eq (2) and (3). The LC of CPs was found to be 31.87% and 46.43% for nanoparticles performed based on the complex coacervation and ionotropic gelation approaches, respectively. Similarly, nanoparticles prepared based on the complex coacervation methodology revealed lower EE level of 73.93%, compared to nanoparticles performed using the ionotropic gelation approach, with EE of 88.54% (**Table 2**). In general, chitosan displays the capability of rapid gelation process upon contact with polyanions, through the creation of inter and intramolecular crosslinking interactions mediated by these polyanions. Consequently, particles are easily shaped subsequently to mixing of TPP and chitosan's amino groups [35].

The LC and EE values obtained in the current study are comparable or even greater when compared against forward obtained data for chitosan−based nanoparticles, prepared by the ionotropic gelation [30,37,38] and complex coacervation [22,39-40] methods, and applied as nanocarriers for hydrophobic drugs/molecules.

3.4. Effective loading of CPs into CS nanoparticles

In the present study, physicochemical characterization techniques involving FTIR and XRD were further adopted to evaluate and confirm the success and the effective loading of CPs into CS nanoparticles.

FTIR spectra of CPs, CS, PI, blank nanoparticles and CPs-loaded nanoparticles, displaying physicochemical interactions are reported in **Fig. 3**. CPs profile showed characteristic bands at 1487 cm^{-1}, 1414 cm^{-1} and 1269 cm^{-1} (aromatic compounds or carboxylic acids, such as phenolic compounds), 1770 cm^{-1} and 1572 cm^{-1} (fatty acid esters and aromatic compounds such as primary amines, respectively), 3002 cm^{-1}, 2944 cm^{-1} and 2864 cm^{-1} (alkyl group from proteins) [42,43]. In fact, CPs are stable complexes, in which the carotenoids are bound to a high-density lipoprotein [44]. For nanoparticles spectra, absorption bands assigned to NH_2 and OH groups stretching vibrations at 3423 cm^{-1}, indicated hydrogen bonding between CS with TPP (ionotropic gelation) and CS with PI (complex coacervation). In addition, bands detected at 1649 cm^{-1}, 1579 cm^{-1}, 1093 cm^{-1}, 894 cm^{-1} corresponded to amide I, amide II, C-O-C and pyranose ring, respectively [28,45]. Upon comparison with unloaded nanoparticles, as a results of hydrogen bonding between CPs and CS, TPP or PI, the band of NH_2-OH group stretching in CPs-loaded nanoparticles has been broadened and shifted to 3374 cm^{-1}, which indicated changes in the CS and PI structure following the encapsulation procedure [5]. The presence of bands at 1566 cm^{-1} and 1420 cm^{-1}, corresponding to C-C aromatic ring in both native CPs as well as CPs-loaded nanoparticles, signposted the successful interaction between CPs, CS and TPP or PI [20,29]. The occurrence of electrostatic forces that act between

positively charged CS nanoparticles and negatively charged CPs, besides the hydrogen bonding and other non-covalent interaction, could be a possible mechanism of interaction between CS and CPs, facilitating its loading. Data abovementioned infers the formation of nanoparticles (ionotropic gelation and complex coacervation) and the effective encapsulation of CPs into them.

Moreover, XRD is a useful tool to explore the nanostructure of matter. Therefore, XRD patterns of CS, blank nanoparticles, and CPs-loaded nanoparticles are presented in **Fig. 4**. CS displayed typical fingerprints of semi-crystalline chitosan, with strong reflections at around 2θ=10.8 ° and 2θ=20.1 °, showing high degree of crystallinity [15]. After electrostatic interaction with TPP (ionotropic gelation) and with PI (complex coacervation), peak alterations and shifts were observed with reduction of peak intensity (**Fig. 4**). Indeed, after cross-linking, no peak was detected in the diffractogram of nanoparticles, reflecting the destruction of the native CS packing structure [20,21]. It is well-known that the width of X-ray diffraction peak is related to the size of crystallite, the broadened peak usually results from imperfect crystal [46]. Consequently, the broad peak of nanoparticles may be caused by the cross-linking reaction between CS and TPP or PI that could destroy the crystalline structure of CS, involving greater disarray in chain alignment in the nanoparticles after complexation [21,31]. In addition, a new peak was found in the diffractogram of nanoparticles at 2θ of around 28 °. These distinct differences reflected the modification in the arrangement of molecules in the crystalline matrix inducted by ionic complexation. Regarding the diffraction spectra of CPs-loaded nanoparticles, compared with the unloaded nanoparticles, the characteristic peak at 2θ of 19 ° confirmed the presence of CPs within nanoparticles. Thus, XRD analysis revealed the successful encapsulation of CPs in nanoparticles, clearly showing the modification in their packing structure.

Accordingly, on behalf of FTIR and XRD data, it is possible to conclude that the two steps emulsion and ionic gelation between CS and TPP (ionotropic gelation), besides complexation between CS and PI (complex coacervation), are suitable for the encapsulation of CPs into nanoparticles [47].

3.5. Thermal characteristics of CPs-loaded nanoparticles

Thermal transition profiles for CS, CPs and nanoparticles from the DSC thermograph allowed to draw further evidences towards the effectiveness of the encapsulation process. DSC thermograms of unloaded and CPs-loaded nanoparticles are shown in **Fig. 5**. The unloaded nanoparticles showed specific prominent peaks ascribed to CS. In fact, an endothermic peak at nearly 100 °C, labeled as dehydration temperature, and a glass transition temperature peak at 202 °C, linked to polymer thermal decomposition [45], were detected. Furthermore, CPs showed a couple of specific melting endotherms at around 100-135 °C that disappeared in CPs-loaded nanoparticles thermograms, regardless the applied encapsulation technique. This could be explained by molecular dispersion of CPs in the polymeric nanoparticles losing its crystallinity, and suggesting thermal stabilization of CPs due to the interaction of CS with TPP (ionotropic gelation) and CS with PI (complex coacervation). This interaction is further substantiated by the absence of any characteristic peaks of PI and TPP.

In addition, the slight reduction in CS dehydration temperature to 85 °C and the lower glass transition temperatures, reaching 198 °C and 177 °C, for the ionotropic gelation and complex coacervation, respectively (**Fig. 5**), reflected the changes involved in the polymer chains order of arrangement upon CPs loading polymeric nanoparticles [30,48].

All the data displayed by the DSC thermographs of the prepared nanoparticles could be correlated with their corresponding TGA curves above described in **Fig. 2**. Accordingly, it could be concluded that the initial melting temperature of CS nanoparticles was effectively enhanced upon CPs encapsulation.

3.6. Morphological characterization of CPs-loaded nanoparticles

The morphology of the nanoparticles was further observed by SEM, since, as above described, the shape and size of particles have strong effect on the fluidity of nanoparticles and thereby their solubility [49]. The SEM images reveal that the size of the blank nanoparticles was higher compared to the CPs-loaded nanoparticles (**Fig. 6**), which is concurrent to the laser scattering particles size distribution findings (**Table 1**). Such characteristic was likewise reported in several studies [50-52]. The swelling of the CS layer adjoining the individual particles, and/or the aggregation of single particles while dispersed in water might be the basis of larger diameter of unloaded nanoparticles [21]. Moreover, more agglomerated particles were observed for unloaded CS nanoparticles (**Fig. 6a (A) and Fig. 6b (A)**), probably as a result of the water absorption behavior of this matrix, generally depending on the chemical properties of surface, and which can be reduced through drying [50]. Conversely, lower agglomerated particles with more uniform appearance were observed for CPs-loaded CS nanoparticles (**Fig. 6a (B) and Fig. 6b (B)**).

In another side, SEM micrographs clearly display that the morphology of the nanoparticles varied significantly depending on the applied formulation method. For both CPs-loaded nanoparticles, the aggregation of particles was further visible, and those aggregates seemed to be melting and combining with each other. As it is shown in **Fig. 6b**, the complex coacervation nanoparticles demonstrated spheroidal shapes and non-smooth surface, likely due to the contribution of PI content with high molecular weight that delay the surface contraction, avoiding the regular spheres formation [51]. Particle morphology of the ionotropic gelation-based nanoparticles (**Fig. 6a**) showed collapsed irregular particles with abundant roughness and cracks on the surface.

Different particle sizes were observed for the nanoparticles, being larger (~ 600 nm) for complex coacervation than those of the ionotropic gelation powder (~ 300 nm). This finding

was in the same line with data of the size measured by the light scattering technique, reflecting that the aggregation or swelling in water of CPs-loaded nanoparticles were lower than those of unloaded nanoparticles, conceivably due to the hydrophobicity of CPs molecules entrapped inside the nanoparticles.

To better study the CPs-loaded CS nanoparticles' microstructure, 3D AFM imaging was performed (**Fig. 7**). Data reveal that CPs-loaded CS nanoparticles prepared by using the ionotropic gelation technique were more uniform in size as compared to CPs-loaded CS nanoparticles based on the complex coacervation approach (**Fig. 7a**). Maximum height of 3.1 nm was observed for ionotropic gelation-based CPs-loaded nanoparticles and 0.21 µm for CS-based nanoparticles according to the complex coacervation method (**Fig. 7b**).

Our findings from SEM and AFM studies demonstrated that the incorporation of CPs decreased significantly the size of CS-based nanoparticles. Further, CS-based nanoparticles unloaded or loaded with CPs prepared by using the ionotropic gelation procedure were smaller and more homogenously dispersed as compared to the complex coacervation-achieved nanoparticles, suggesting that CPs could behave like surfactant by additional increase of the dispersity and thereby CS-based nanoparticles' surface area [49].

3.7. Stability study of CPs-loaded CS nanoparticles

Lyophilized CPs-loaded CS nanoparticles were subjected to stability studies at 80, 100 and 120 °C (sterilization temperatures) for 5, 15 and 30 min. Particle size (**Fig. 8a**) and zeta potential (**Fig. 8b**) were determined at each desired time interval.

Droplet size diameter is reported to be a key factor able of physical stability illustration and physicochemical behavior modification of encapsulated compounds [53]. As shown in **Fig. 8a**, whatever the encapsulation method used, the particle diameter of CPs loaded nanoparticles increased significantly with the increase of heat time from 5 to 30 min and temperature from 80 to 120 °C ($p<0.05$). Indeed, size values increased from 5.4 µm to 10.45 µm after an

incubation time of 30 min at 80 °C, and to 10.73 after a 30 min incubation time at 120 °C, in the case of the complex coacervation process (**Fig. 8a (A)**). This finding implies an increase in the number of larger particles and a decrease in the narrow distribution of the suspension size, and thereby, its meager thermal stability. In fact, there is an intensification in particles' collision frequency, typically under heat treatment, and thereafter the unfold of proteins present within the particles, which could uphold particles aggregation [54]. In addition, nanoparticles size revealed a significant increase with temperature augmentation, which could be assigned to PI denaturation, regarding the CS-PI based nanoparticles, promoting the aggregation of nanoparticles due to modifications in their configuration, triggered by higher temperatures [55].

Conversely, the particle size of CPs loaded nanoparticles prepared via the ionotropic gelation approach was smaller after a 30 min heating reaction time at 120 °C (10.01 µm) ($p<0.05$). This finding interestingly demonstrated that CS crosslinked with TPP protected CPs molecules from heat-induced aggregation (**Fig.8a (B)**). Moreover, CPs loaded nanoparticles prepared by ionotropic gelation were found to exhibit a good heat-stability at 80 °C. In fact, it has been previously reported that CS nanoparticles exhibited an increase in particle size during storage, mainly due to the swelling, the aggregation of the particles and the interaction of the chains of free polymers with the particles network [56].

In another side, zeta potential data, often considered as particle suspensions and colloidal samples stability sign, were recovered (**Fig. 8b**). Indeed, a high zeta potential (either positive or negative) is required to maintain particle distance and protect their stability, allowing a sufficient repulsive energy [49,54]. Indeed, a low zeta potential value (almost null) led to faster particles coagulation and sedimentation. Nevertheless, at high zeta potential, electrostatic repulsion forces between particles allow the improvement of their stability. Thus, micro-systems moderate stability is observed with zeta potential around ± 30 mV, good stability at around ± 50 mV and excellent stability at zeta potential value ≥ ± 60 mV [57]. It is worthy to

mention that zeta potential of heated CPs-loaded nanoparticles was decreasing with the rise of heating temperature and incubation time (**Fig. 8b**). Despite this decrease, data from zeta potential analysis suggest that the tested nano-carriers prepared by ionotropic gelation and complex coacervation should be sufficiently stable against heat with average zeta potential more than +30 mV in both cases.

Findings regarding heat resistance of CPs-loaded nanoparticles corroborate well with above mentioned results in the present study. In fact, lower encapsulation efficiency might indicate that there is too much uncapsulated core on the nanoparticle's surface [22,34], as perceived in complex coacervation-based nanoparticles, which can explain its lower stability. Compared to ionotropic gelation, the achieved nanoparticles better stability can be ascribed to Tween-80, used as non-ionic surfactant that delays the establishment of aggregates, promoting thereby the formation of CPs-loaded nanoparticles.

Overall results in the present study suggest that, due its cross-linking effect, stimulating polymeric molecules to create tougher interactions with each other, TPP acts as stabilizer, improving nanoparticles structural stability. Subsequently, CS-TPP, as nanocarrier, could be adopted as a tool to protect active and sensible molecules against oxidation.

3.8. *In vitro* release kinetics assessments of CPs from CS nanoparticles

It is well known that drug or biomolecules release from nanoparticles take place by several mechanisms, including surface erosion, disintegration, diffusion and desorption [16,18]. The *in vitro* release study of CPs from prepared nanoparticles was subsequently monitored to understand and to recognize the release mechanism and kinetics of CPs, which is decisive for ulterior applications of CPs-loaded nanocarriers [8,58].

The *in vitro* release profiles of CPs from the nanoparticles are reported in **Fig. 9**, considering the amount of CPs released as function of different times, measured at 480 nm, based on a calibration curve of CPs concentration (**Data not shown**). The *in vitro* release

scheme of CPs from nanoparticles can be labelled as a biphasic process (**Fig. 9**), with an initial rapid release followed by subsequent slower release. The initial swift release was attributed to the CPs molecules entrapped near the surface, where the dissolution rate of the polymer near the surface is high [21,37,59]. In the second stage, the release rate was rather slow, attaining a plateau, probably due to the diffusion of the CPs dispersed into the CS matrix as the dominant mechanism, and thus, nearly no further release of CPs (**Fig. 9**). Supplementary release of CPs required the swelling and/or degradation of the compact CS-TPP and CS-PI nanoparticles.

Similar results of encapsulated materials were reported with chitosan nanoparticles, with swift initial release followed subsequently by a slow release [5,14,22,49]. It is important to pointed out that the deliverance of a drug by diffusion related the swelling and the transformation from glassy into rubbery polymer matrix, as a result of the penetration of medium into the particle system [2,60].

In the present study, two media were used, ethanol and PBS (pH~6.8), as CPs are dissolved well in both solvents. The release shapes of CPs in ethanol and PBS were to variable extend analogous, with the typical biphasic delivery process. Otherwise, the release of CPs in ethanol reached a plateau within 90 min (ionotropic gelation) and 150 min (complex coacervation). Nonetheless, reaching a plateau in PBS, required a shorter time, such as 30 min (ionotropic gelation) and 90 min (complex coacervation). This might be an outcome of the weakening of the electrostatic interaction between the cationic carrier (CS) and anionic TPP (inotropic gelation) or PI (complexe coacervation), resulting in faster and shorter release time. Due to the higher solubility of CPs in ethanol, the quantity of CPs released in ethanol was higher than that in PBS.

In terms of the encapsulation methodology, the amount of CPs released from nanoparticles prepared by ionotropic gelation (**Fig. 9a**) was found to be greater, with shorter release interval than that of nanoparticles prepared using the complex coacervation approach

(**Fig. 9b**). In fact, mainly due to better surface-to-volume ratio, nanoparticles with reduced particle size may result in an easy and fast deliverance of entrapped CPs. Furthermore, the quantity of released CPs was found to be modulated by the amount of CPs entrapped. In fact, the high LC, reaching more than 46% with the ionotropic gelation process *vs.* ~32% for the complex coacervation **(Table 2)**, provided a fast release rate and a concomitantly high amount of released CPs [28].

Hereafter, data in the present research indicate that the CS based nano-systems, engineered by the ionotropic gelation and complex coacervation, are suitable for controlling the release of CPs.

4. Conclusion

CPs-loaded nanoparticles were successfully prepared by complex coacervation and ionotropic gelation approaches, as confirmed by FTIR, TGA/DTG and XRD analytical techniques. The nanoparticles were spherical in shape with positively charged surfaces and size depending on the formulation approach, where ionotropic gelation allowed the development of smaller nanoparticles, with higher LC and EE. The *in vitro* release studies indicated that the content of encapsulated CPs influenced its release rate from nanoparticles, with higher released CPs and shorter release interval, adopting the ionotropic gelation approach. Therefore, the effectiveness of CS-TPP, as a nano-carrier biopolymer for encapsulating bioactive substances, and its potential use in several fields, namely for drug delivery. Moreover, the good thermal stability of CS-PI nanoparticules, obtained by complex coacervation, signposted that CS-PI coacervate could be suitable to be used for encapsulation of thermally sensitive materials.

Acknowledgement

The present work was funded by the Ministry of Higher Education and Scientific Research, Tunisia. The authors thank Dr. Mohamed Ayman KAMMOUN for his aid regarding the realization of the AFM analysis.

References

1. A., Menin, F., Zanoni, M., Vakarelova, R., Chignola, G., Donà, C., Rizzi, F., Mainente, G. Zoccatelli (2018). Effects of microencapsulation by ionic gelation on the oxidative stability of flaxseed oil. *Food Chemistry*, 269, 293-299.
2. Y.F., Tan, L.L., Lao, G.M., Xiong, S. Venkatraman (2018). Controlled-release nanotherapeutics: State of translation. *Journal of Controlled Release*, 284, 39–48.
3. Y.A., Skorik, A.A., Golyshev, A.S., Kritchenkov, E.R., Gasilova, D.N., Poshina, A.J., Sivaram, R. Jayakumar (2017). Development of drug delivery systems for taxanes using ionic gelation of carboxyacyl derivatives of chitosan. *Carbohydrate Polymers*, 162, 49-55.
4. E., Yilmaz, Z., Yalinca, K., Yahya, U. Sirotina (2016). pH responsive graft copolymers of chitosan. *International Journal of Biological Macromolecules*, 90, 68–74.
5. T., Wu, C., Wu, S., Fu, L., Wang, C., Yuan, S., Chen, Y. Hu (2017). Integration of lysozyme into chitosan nanoparticles for improving antibacterial activity. *Carbohydrate Polymers*, 155, 192–200.
6. P., Huang, X., Wang, X., Liang, J., Yang, C., Zhang, D., Kong, W. Wang, (2019). Nano-, micro-, and macroscale drug delivery systems for cancer immunotherapy. *Acta Biomaterialia*, 85, 1-26.
7. D., Eratte, K., Dowling, C.J., Barrow, B. Adhikari, (2018). Recent advances in the microencapsulation of omega-3 oil and probiotic bacteria through complex coacervation: A review. *Trends in Food Science & Technology*, 71, 121-131.
8. F.L., Tulini, V.B., Souza, M., Thomazini, M.P., Silva, A.P., Massarioli, S.M., Alencar, E.M.J.A., Pallone, M.I., Genovese, C.S. Favaro-Trindade, (2017). Evaluation of the release profile, stability and antioxidant activity of a proanthocyanidin-rich cinnamon (Cinnamomum zeylanicum) extract co-encapsulated with α-tocopherol by spray chilling. *Food Research International*, 95, 117-124.
9. D.I., Sánchez-Machado, J., López-Cervantes, M.A., Correa-Murrieta, R.G., Sánchez-Duarte, P., Cruz-Flores, G.S. de la Mora-López, (2019). Chitosan. *Nonvitamin and Nonmineral Nutritional Supplements*, 485-493.
10. N., Alves, J., Mano, (2008). Chitosan derivatives obtained by chemical modifications for biomedical and environmental applications. *International Journal of Biological Macromolecules*, 43, 401–414.
11. E., Vunain, A.K., Mishra, B.B. Mamba, (2017). Fundamentals of chitosan for biomedical applications. *Chitosan Based Biomaterials Volume 1 – Fundamentals*, 3-30.

12. S., Ketnawa, O., Martinez-Alvarez, J., Gomez-Estaca, M.C., Gomez-Guillen, S., Benjakul, S., Rawdkuen, (2016). Obtaining of functional components from cooked shrimp (*Penaeus vannamei*) by enzymatic hydrolysis. *Food Bioscience*, 15, 55–63.

13. B., Wang, B., Adhikari, C.J. Barrow, (2018). Highly stable spray dried tuna oil powders encapsulated in double shells of whey protein isolate-agar gum and gellan gum complex coacervates. *Powder Technology*, In Press, Corrected proof.

14. F., Duman, M. Kaya, (2016). Crayfish chitosan for microencapsulation of coriander (*Coriandrum sativum* L.) essential oil. *International Journal of Biological Macromolecules*, 92, 125–133.

15. M., Hamdi S., Hajji S., Affes W., Taktak H., Maâlej M., Nasri R. Nasri (2018a). Development of a controlled bioconversion process for the recovery of chitosan from blue crab (*Portunus segnis*) exoskeleton. *Food Hydrocolloids*, 77, 534-548.

16. M., Hamdi, R., Nasri, N., Dridi, H., Moussa, L., Ashour, M. Nasri (2018b). Improvement of the quality and the shelf life of reduced-nitrites turkey meat sausages incorporated with carotenoproteins from blue crabs' shells. *Food Control*, 91, 148-159.

17. M., Chaijan, W., Panpipat, S. Benjakul, (2010). Physicochemical and gelling properties of short-bodied mackerel (Rastrelliger brachysoma) protein isolate prepared using alkaline-aided process. *Food and Bioproducts Processing*, 88, 174-180.

18. P.G., Chang, R., Gupta, Y.P., Timilsena, B. Adhikari (2016). Optimisation of the complex coacervation between canola protein isolate and chitosan. *Journal of Food Engineering*, 191, 58-66.

19. G.Q., Huang, Y.T., Sun, J.X., Xiao, J. Yang, (2012). Complex coacervation of soybean protein isolate and chitosan. *Food Chemistry*, 135, 534–539.

20. J., Haider, H., Majeed, P.A., Williams, W., Safdar, F. Zhong, (2017). Formation of chitosan nanoparticles to encapsulate krill oil (*Euphausia superba*) for application as a dietary supplement. *Food Hydrocolloids*, 63, 27-34.

21. R., Yoksan, J., Jirawutthiwongchai, K. Arpo, (2010). Encapsulation of ascorbyl palmitate in chitosan nanoparticles by oil-in-water emulsion and ionic gelation processes. *Colloids and Surfaces B: Biointerfaces*, 76, 292–297.

22. M.C.R., da Cruz, J.L.A., Dagostin, C.A., Perussello, M.L. Masson, (2019). Assessment of physicochemical characteristics, thermal stability and release profile of ascorbic acid microcapsules obtained by complex coacervation. *Food Hydrocolloids*, 87, 71–82.

23. E.F., de Matos, B.S., Scopel, A. Dettmer, (2018). Citronella essential oil microencapsulation by complex coacervation with leather waste gelatin and sodium alginate. *Journal of Environmental Chemical Engineering*, 6, 1989-1994.

24. N., Eghbal, R. Choudhary, (2018). Complex coacervation: Encapsulation and controlled release of active agents in food systems. *LWT – Food Science and Technology*, 90, 254-264.

25. A., Jain, D., Thakur, G., Ghoshal, O.P., Katare, U.S. Shivhare, (2016). Characterization of microcapsulated β-carotene formed by complex coacervation using casein and gum tragacanth. *International Journal of Biological Macromolecules*, 87, 101-113.

26. E., Duhoranimana, J., Yu, O., Mukeshimana, I., Habinshuti, E., Karangwa, X., Xu, B., Muhoza, S., Xia, X. Zhang, (2018). Thermodynamic characterization of gelatin–sodium carboxymethyl cellulose complex coacervation encapsulating conjugated linoleic acid (CLA). *Food Hydrocolloids*, 80, 149-159.

27. S.A., Agnihotri, T.M. Aminabhavi, (2006). Novel interpenetrating network chitosan-poly(ethylene oxide-g-acrylamide) hydrogel microspheres for the controlled release of capecitabine. *International Journal of Pharmaceutics*, 324, 103-115.

28. S.C.S.R., de Moura, C.L., Berling, S.P.M., Germer, I.D., Alvim, M.D. Hubinger, (2017). Encapsulating anthocyanins from *Hibiscus sabdariffa* L. calyces by ionic gelation: Pigment stability during storage of microparticles. *Food Chemistry*, 241, 317-327.

29. D., Arora, V., Dhanwal, D., Nayak, A., Saneja, H., Amin, R., Rasool, P., Narayan Gupta, A. Goswami, (2016). Preparation, characterization and toxicological investigation of copper loaded chitosan nanoparticles in human embryonic kidney HEK-293 cells. *Materials Science and Engineering C*, 61, 227–234.

30. R., Panwar, S.C., Pemmaraju, A.K., Sharma, V. Pruthi, (2016). Efficacy of ferulic acid encapsulated chitosan nanoparticles against Candida albicans biofilm. *Microbial Pathogenesis*, 95, 21-31.

31. S., Anandhakumar, G., Krishnamoorthy, K.M., Ramkumar, A.M. Raichur, (2017). Preparation of collagen peptide functionalized chitosan nanoparticles by ionic gelation method: An effective carrier system for encapsulation and release of doxorubicin for cancer drug delivery. *Materials Science and Engineering C*, 70, 378–385.

32. A., Reznickova, N., Slavikova, Z., Kolska, K., Kolarova, T., Belinova, M., Hubalek Kalbacova, M., Cieslar, V. Svorcik, (2018). PEGylated gold nanoparticles: stability, cytotoxicity and antibacterial activity. *Colloids and Surfaces A: Physicochemical and Engineering Aspects*, 560, 26-34.

33. P., Bagre, K., Jain, N.K. Jain, (2013). Alginate coated chitosan core shell nanoparticles for oral delivery of enoxaparin: *In vitro* and *in vivo* assessment. *International Journal of Pharmaceutics*, 456, 31-40.

34. K.I., Jang, H.G. Lee, (2008). Stability of chitosan nanoparticles for L ascorbic acid during heat treatment in aqueous solution. *Journal of Agricultural and Food Chemistry*, 56, 1936-1941.

35. S., Woranuch, R. Yoksan, (2013). Eugenol-loaded chitosan nanoparticles: I. Thermal stability improvement of eugenol through encapsulation. *Carbohydrate Polymers*, 96, 578-585.

36. J., Zhu, M., Xiao, X., Zhao, C., Liu, W. Xing, (2015). Titanium dioxide encapsulated in nitrogen-doped carbon enhances the activity and durability of platinum catalyst for Methanol electro-oxidation reaction. *Journal of Powder Sources*, 292, 78-86.

37. M., Ghaderi-Ghahfarokhi, M., Barzegar, M.A., Sahari, H., Ahmadi Gavlighi, F. Gardini, (2017). Chitosan-cinnamon essential oil nano-formulation: Application as a novel additive for controlled release and shelf life extension of beef patties. *International Journal of Biological Macromolecules*, 102, 19-28.

38. S.F., Hosseini, M., Zandi, M., Rezaei, F. Farahmandghavi, (2013). Two-step method for encapsulation of oregano essential oil in chitosan nanoparticles: Preparation, characterization and in vitro release study. *Carbohydrate Polymers*, 95, 50-56.

39. N.D., Gonçalves, C.R.F., Grosso, R.S., Rabelo, M.D., Hubinger, A.S. Prata, (2018). Comparison of microparticles produced with combinations of gelatin, chitosan and gum Arabic. *Carbohydrate Polymers*, 196, 427-432.

40. X., Huo, W., Li, Y., Wang, N., Han, J., Wang, N., Wang, X. Zhang, (2018). Chitosan composite microencapsulated comb-like polymeric phase change material via coacervation microencapsulation. *Carbohydrate Polymers*, 200, 602-610.

41. L., Shi, S.K., Beamer, H., Yang, J. Jaczynski, (2018). Micro-emulsification/encapsulation of krill oil by complex coacervation with krill protein isolated using isoelectric solubilization/precipitation. *Food Chemistry*, 244, 284–291.

42. H.L., Liu, B.H., Chen, T.H., Kao, C.Y. Shiau, (2014). Carotenoids composition in Scultellaria barbata D. as detected by high performance liquid chromatography-diode array detection-mass spectrometry-atmospheric pressure chemical ionization. *Journal of Functional Foods*, 8, 100-110.

43. N., Mezzomo, B., Maestri, R.L., dos Santos, M., Maraschin, S.R.S. Ferreira, (2011). Pink shrimp (P. brasiliensis and P. paulensis) residue: Influence of extraction method on carotenoid concentration. *Talanta*, 85, 1383–1391.

44. T., Senphan, S., Benjakul, H. Kishimura, (2014). Characteristics and Antioxidative activity of carotenoproteins from shells of Pacific white shrimp extracted using hepatopancreas proteases. *Food Bioscience*, 5, 54–63.

45. A., Rampino, M., Borgogna, B., Bellich, P., Blasic, F., Virgilio, A. Cesàro, (2016). Chitosan-pectin hybrid nanoparticles prepared by coating and blending techniques. *European Journal of Pharmaceutical Sciences*, 84, 37-45.

46. J., Ji, S., Hao, D., Wu, R., Huang, Y. Xu, (2011). Preparation, characterization and in vitro release of chitosan nanoparticles loaded with gentamicin and salicylic acid. *Carbohydrate Polymers*, 85, 803-808.

47. C., Xu, L., Cao, P., Zhao, Z., Zhou, C., Cao, F., Li, Q. Huang (2018). Emulsion-based synchronous pesticide encapsulation and surface modification of mesoporous silica nanoparticles with carboxymethyl chitosan for controlled azoxystrobin release. *Chemical Engineering Journal*, 348, 244-254.

48. L., Keawchaoon, R. Yoksan, (2011). Preparation, characterization and in vitro release study of carvacrol-loaded chitosan nanoparticles. *Colloids and Surfaces B: Biointerfaces*, 84, 163-171.

49. M.K., Yeh, K.M., Cheng, C.S., Hu, Y.C., Huang, J.J. Young, (2011). Novel protein-loaded chondroitin sulfate–chitosan nanoparticles: Preparation and characterization. *Acta Biomaterialia*, 7, 3804-3812.

50. M.C., Otálora, J.G., Carriazo, C., Osorio, M.A. Nazareno, (2018). Encapsulation of cactus (Opuntia megacantha) betaxanthins by ionic gelation and spray drying: A comparative study. *Food Research International*, 111, 423-430.

51. B., Jamil, H., Habib, S., Abbasi, H., Nasir, A., Rahman, A., Rehman, H., Bokhari, M. Imran, (2016). Cefazolin loaded chitosan nanoparticles to cure multi drug resistant Gram-negative pathogens. *Carbohydrate Polymers*, 136, 682-691.

52. R.A., Hashad, R.A.H., Ishak, A.S., Geneidi, S. Mansour (2016). Methotrexate loading in chitosan nanoparticles at a novel pH: Response surface modeling, optimization and characterization. *International Journal of Biological Macromolecules*, 91, 630–639.

53. M., Benjemaa, M.A., Neves, H., Falleh, H., Isoda, R., Ksouri, M. Nakajima (2018). Nanoencapsulation of *Thymus capitatus* essential oil: Formulation process, physical stability

characterization and antibacterial efficiency monitoring. *Industrial Crops & Products*, 113, 414–421.

54. C., de Campo, M., Dick, P.P., dos Santos, T.M.H., Costa, K., Paese, S.S., Guterres, A., de Oliveira Rios, S. Hickmann Flores (2018). Zeaxanthin nanoencapsulation with *Opuntia monacantha* mucilage as structuring material: characterization and stability evaluation under different temperatures. *Colloids and Surfaces A: Physicochemical and Engineering Aspects*, 558, 410-421.

55. B., Jin, X., Zhou, Y., Liu, X., Li, Y., Mai, Y., Liao, J. Liao (2018). Physicochemical stability and antioxidant activity of soy protein/pectin/tea polyphenol ternary nanoparticles obtained by photocatalysis. *International Journal of Biological Macromolecules*, 116, 1-7.

56. S., Rodrigues, A.M.R., da Costa, A. Grenha (2012). Chitosan/carrageenan nanoparticles: Effect of cross-linking with tripolyphosphate and charge ratios. *Carbohydrate Polymers*, 89, 282– 289.

57. A., Reznickova, N., Slavikova, Z., Kolska, K., Kolarova, T., Belinova, M., Hubalek Kalbacova, M., Cieslar, V. Svorcik, (2018). PEGylated gold nanoparticles: stability, cytotoxicity and antibacterial activity. *Colloids and Surfaces A: Physicochemical and Engineering Aspects*, 560, 26-34.

58. C., Wyatt Shields IV, J.P., White, E.G., Osta, J., Patel, S., Rajkumar, N., Kirby, J.P., Therrien, S. Zauscher (2018). Encapsulation and controlled release of retinol from silicone particles for topical delivery. *Journal of Controlled Release*, 278, 37-48.

59. A.M., Thomas, A., Kapanen, J.I., Hare, E., Ramsay, K., Edwards, G., Karlsson, M.B. Bally, (2011). Development of a liposomal nanoparticle formulation of 5-Fluorouracil for parenteral administration: Formulation design, pharmacokinetics and efficacy. *Journal of Controlled Release*, 150, 212-219.

60. B., Wang, B., Adhikari, C.J. Barrow, (2014). Optimisation of the microencapsulation of tuna oil in gelatin–sodium hexametaphosphate using complex coacervation. *Food Chemistry*, 158, 358-365.

Figure captions

Figure 1: Zeta potential of PI, CS and CS-PI coacervates, and strength of electrostatic force (SEI) **(A).** Complex coacervates yield and turbidity *vs.* pH **(B)**. Turbidity and the yield of complex coacervates at pH 6.0 with different PI-CS mass ratios **(C)**.

Figure 2: **(a)** ATG thermograms of nanoparticles via ionotropic gelation **(A)** and complex coacervation **(B)**. **(b)** DTG thermograms of CS-based microcapsules via ionotropic gelation **(A)** and complex coacervation **(B)**.

Figure 3: ATR-FTIR spectra of nanoparticles via ionotropic gelation **(A)** and complex coacervation **(B)**.

Figure 4: XRD patterns of nanoparticles prepared via ionotropic gelation **(A)** and complex coacervation **(B)**.

Figure 5: DSC profiles of CS-based microcapsules via ionotropic gelation **(A)** and complex coacervation **(B)**.

Figure 6: **a)** SEM imaging of unloaded **(A)** and CPs-loaded **(B)** nanoparticles via ionotropic gelation. **b)** SEM imaging of unloaded **(A)** and CPs-loaded **(B)** nanoparticles via complex coacervation.

Figure 7: **a)** AFM images of **(A)** surface topographic and phase, and **(B)** 3D image of unloaded CPs-loaded nanoparticles prepared by using the ionotropic gelation procedure. **b)** Surface topographic and phase **(A)**, and **(B)** 3D image of CPs-loaded nanoparticles elaborated according to the complex coacervation method, at 2×2 µm area.

Figure 8: Particle size **(a)** and zeta potential **(b)** evolution *vs.* temperature and incubation time of CPs-loaded nanoparticles using ionotropic gelation **(A)** and complex coacervation **(B)**.

Figure 9: *In vitro* release assessments of CPs from nanoparticles prepared using ionotropic gelation **(A)** and complex coacervation **(B)**.

Fig. 1

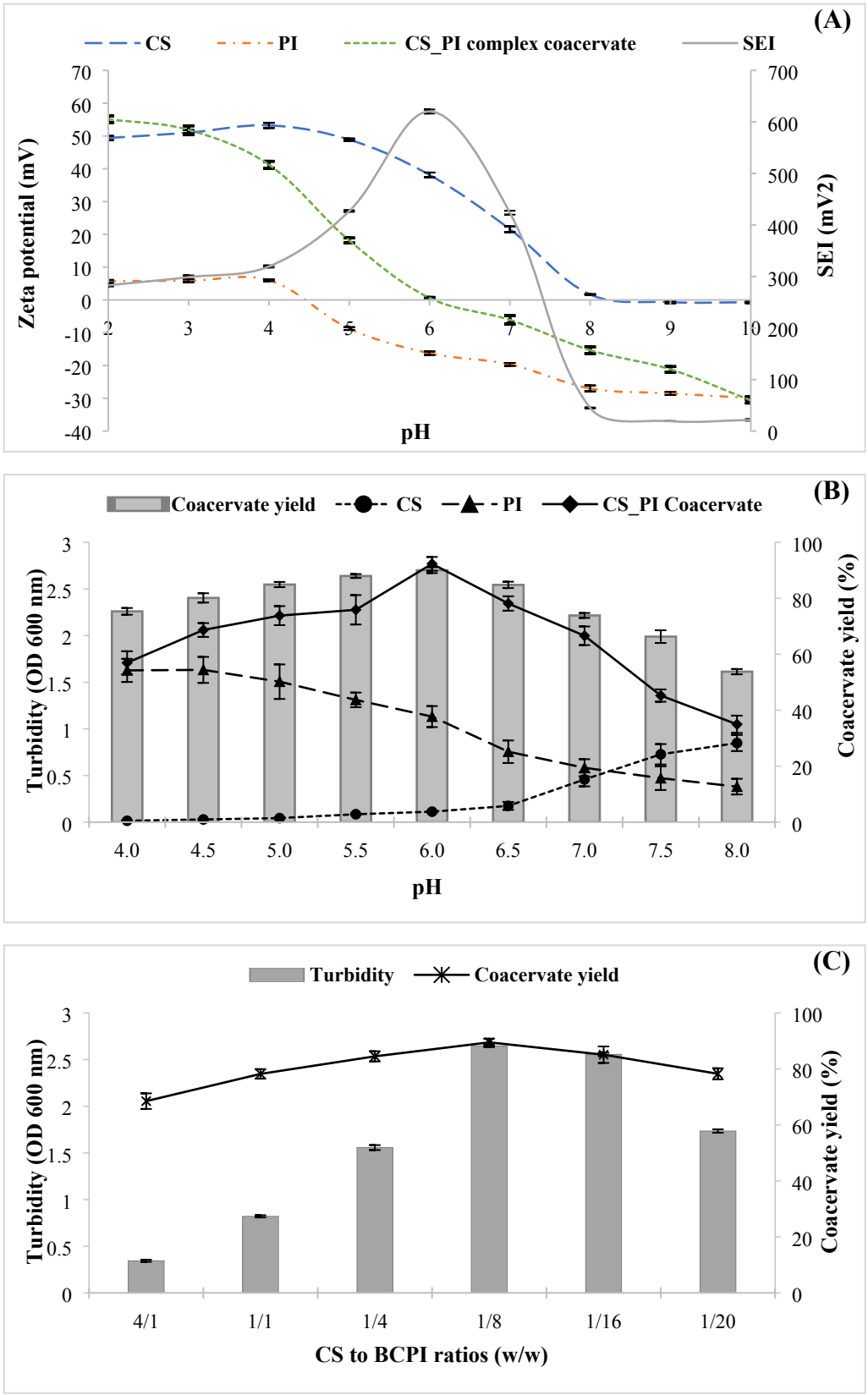
(A)
CS
PI
CS_PI complex coacervate
SEI
Zeta potential (mV)
SEI (mV2)
pH
(B)
Coacervate yield
CS
PI
CS_PI Coacervate
Turbidity (OD 600 nm)
Coacervate yield (%)
pH
(C)
Turbidity
Coacervate yield
Turbidity (OD 600 nm)
Coacervate yield (%)
4/1
1/1
1/4
1/8
1/16
1/20
CS to BCPI ratios (w/w)

Fig. 2

(a)

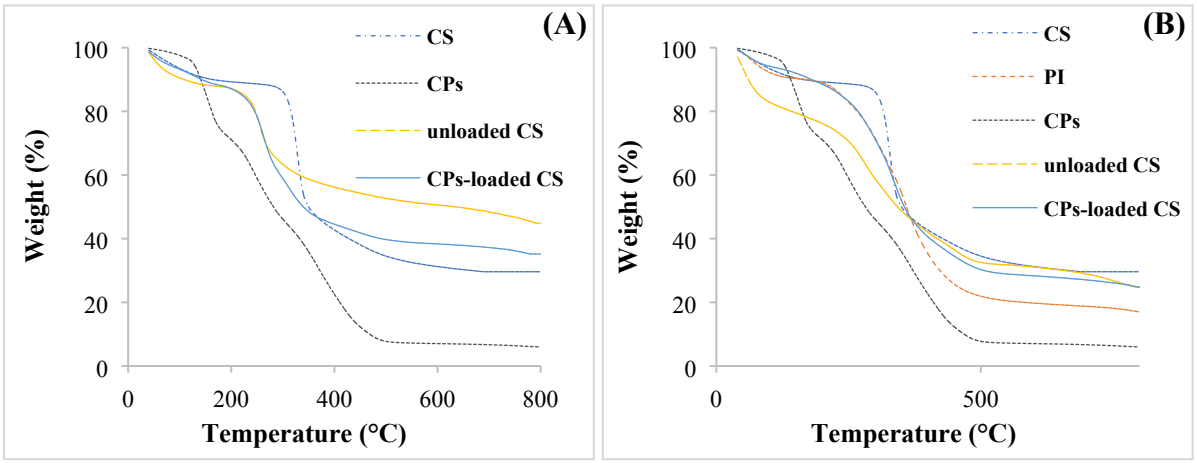
(A)
CS
CPs
unloaded CS
CPs-loaded CS
Weight (%)
100
80
60
40
20
0
0
200
400
600
800
Temperature (°C)
(B)
CS
PI
CPs
unloaded CS
CPs-loaded CS
Weight (%)
100
80
60
40
20
0
0
500
Temperature (°C)

(b)

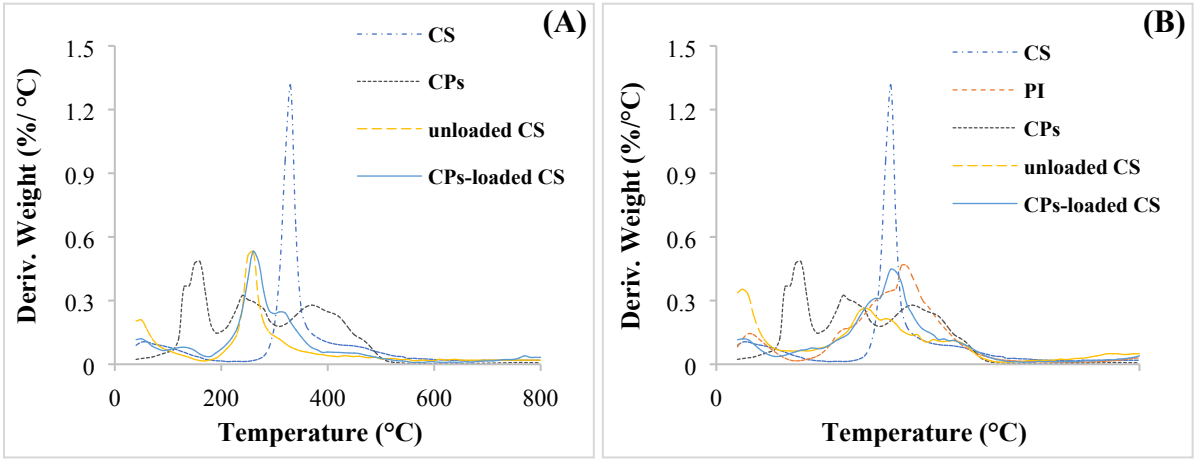
(A)
CS
CPs
unloaded CS
CPs-loaded CS
Deriv. Weight (%/ °C)
1.5
1.2
0.9
0.6
0.3
0
0
200
400
600
800
Temperature (°C)
(B)
CS
PI
CPs
unloaded CS
CPs-loaded CS
Deriv. Weight (%/°C)
1.5
1.2
0.9
0.6
0.3
0
0
Temperature (°C)

Fig. 3

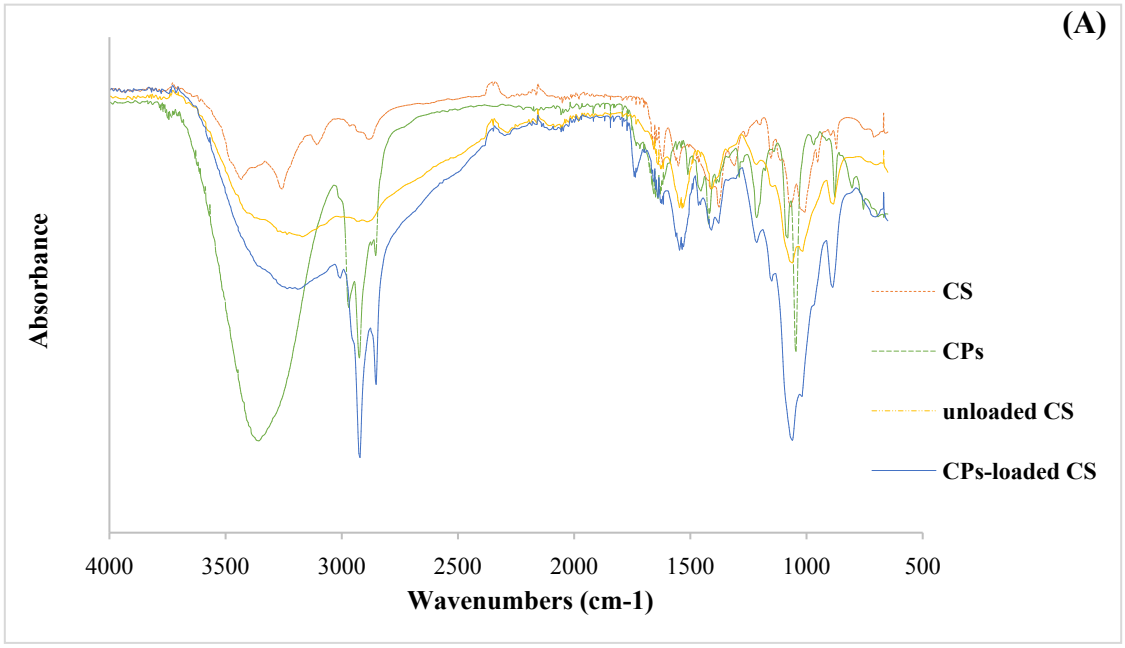
(A)
Absorbance
4000
3500
3000
2500
2000
1500
1000
500
Wavenumbers (cm-1)
CS
CPs
unloaded CS
CPs-loaded CS

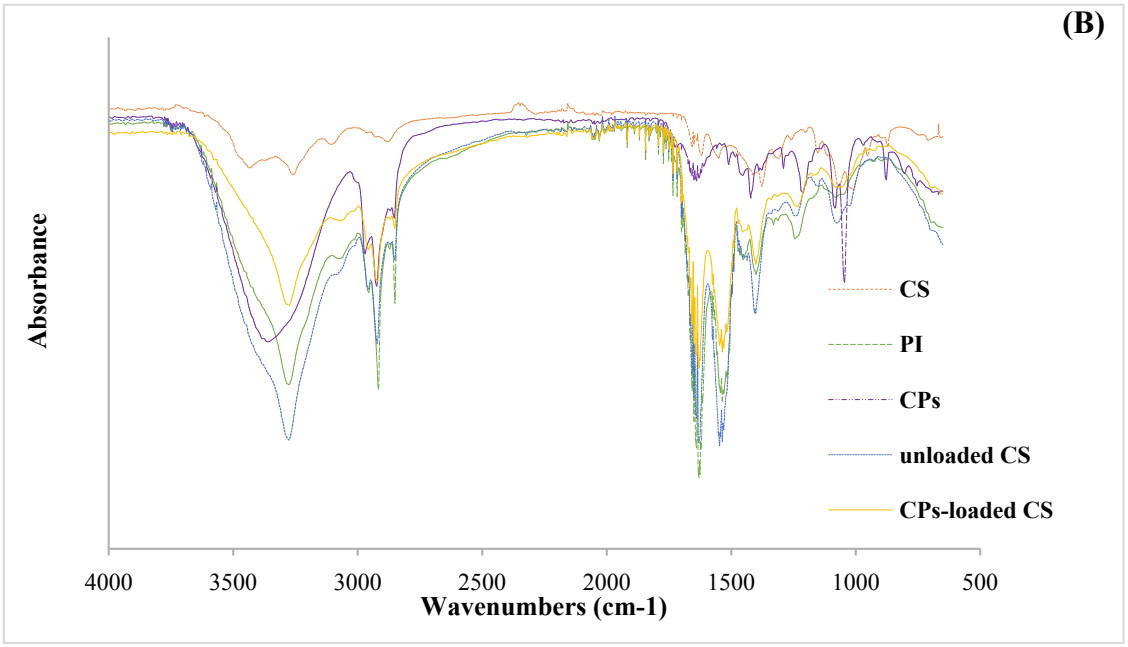
(B)
Absorbance
4000
3500
3000
2500
2000
1500
1000
500
Wavenumbers (cm-1)
CS
PI
CPs
unloaded CS
CPs-loaded CS

Fig. 4

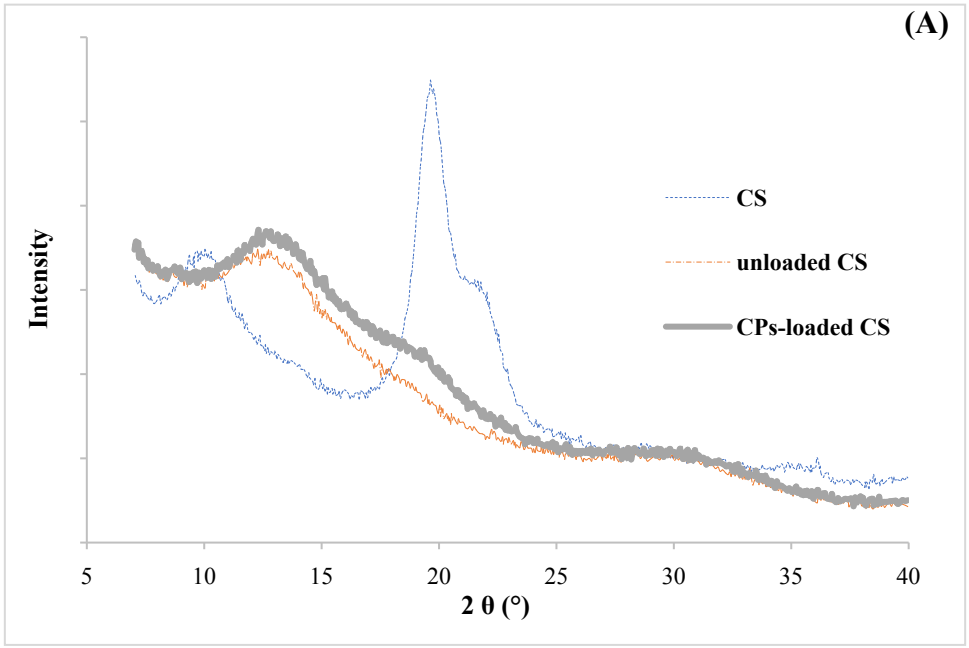
(A)
Intensity
CS
unloaded CS
CPs-loaded CS
5
10
15
20
25
30
35
40
2 θ (°)

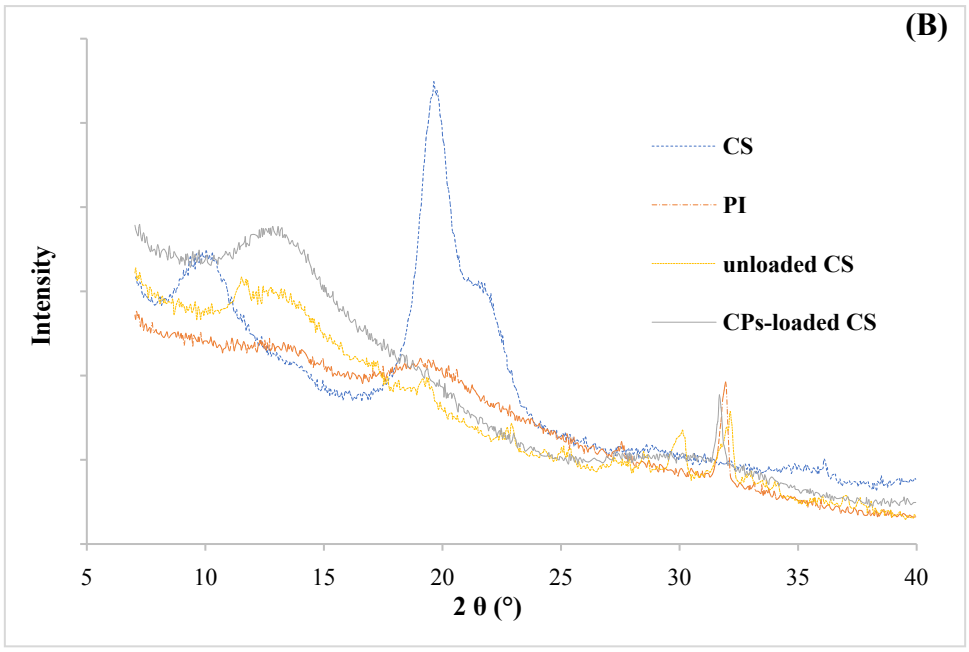
(B)
Intensity
CS
PI
unloaded CS
CPs-loaded CS
5
10
15
20
25
30
35
40
2 θ (°)

Fig. 5

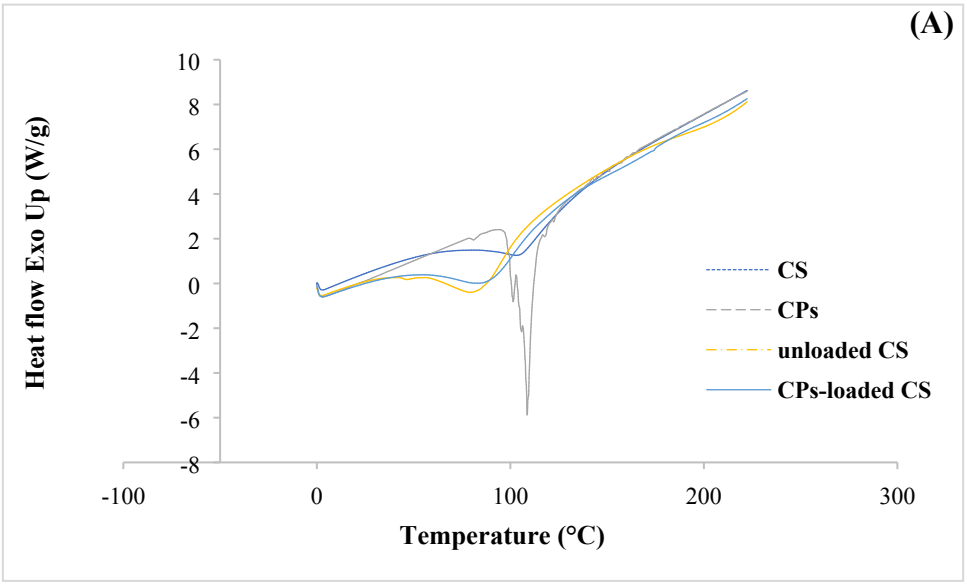
(A)
Heat flow Exo Up (W/g)
10
8
6
4
2
0
-2
-4
-6
-8
-100
0
100
200
300
Temperature (°C)
CS
CPs
unloaded CS
CPs-loaded CS

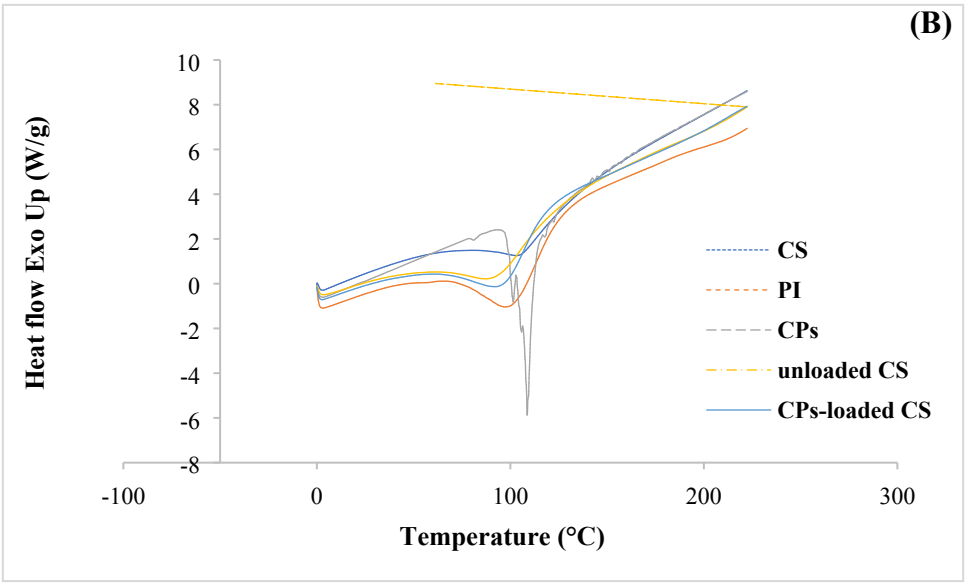
(B)
Heat flow Exo Up (W/g)
10
8
6
4
2
0
-2
-4
-6
-8
-100
0
100
200
300
Temperature (°C)
CS
PI
CPs
unloaded CS
CPs-loaded CS

Fig. 6

(a) **A** **B**

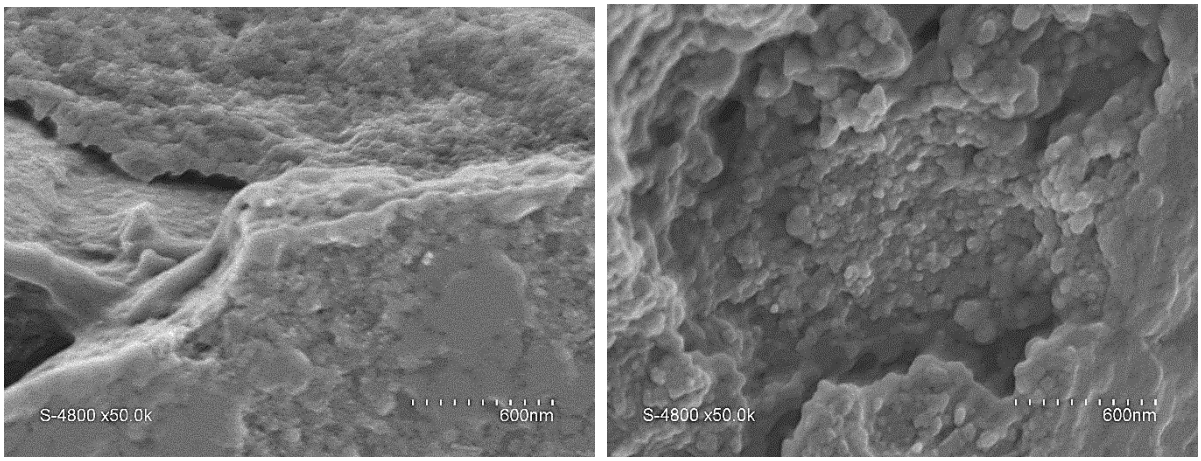
S-4800 x50.0k
600nm
S-4800 x50.0k
600nm

(b) **A** **B**

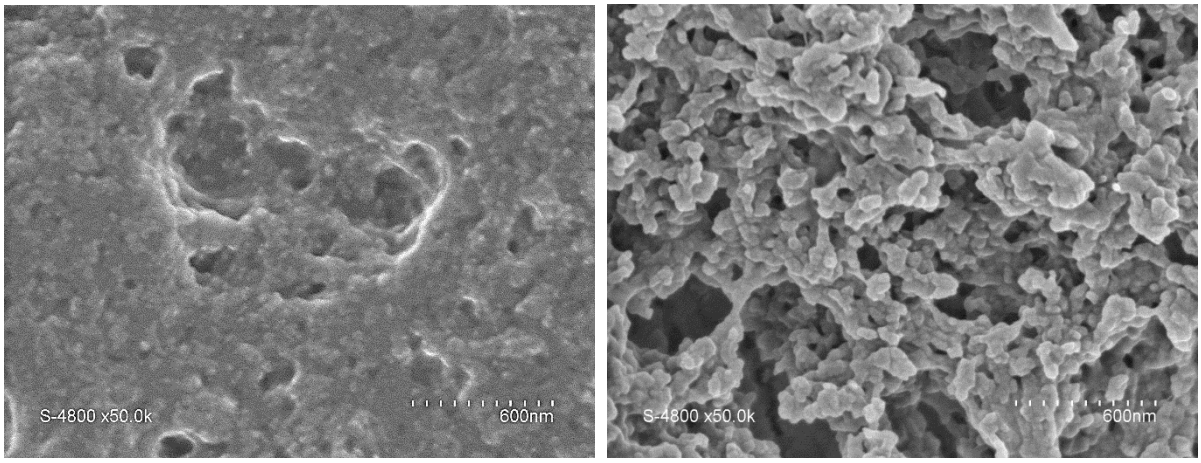
S-4800 x50.0k
600nm
S-4800 x50.0k
600nm

Fig. 7

A

Ionotropic Gelation **Complex Coacervation**

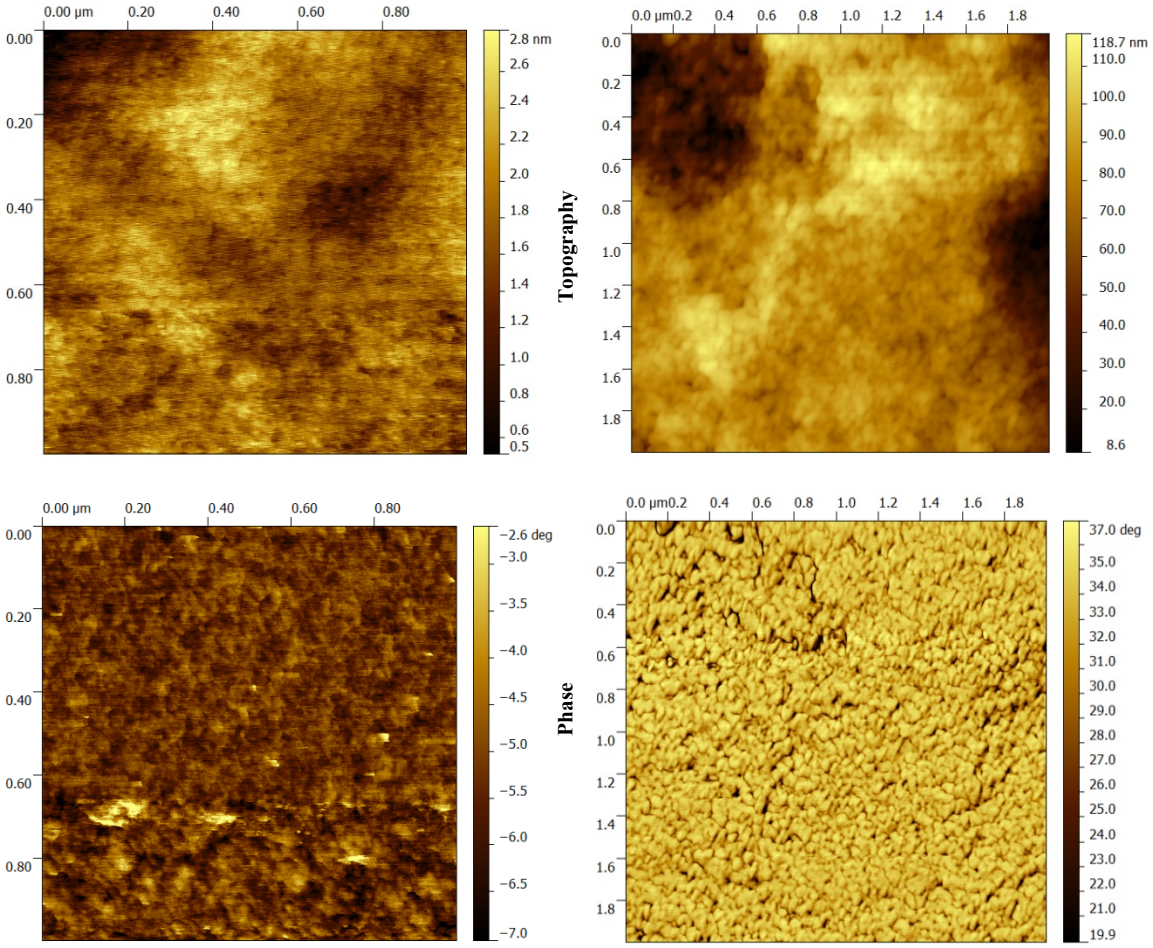

B

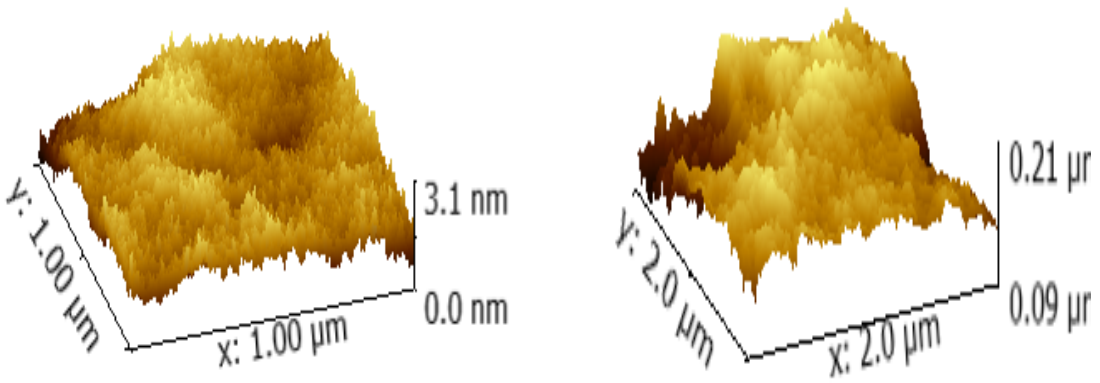

Fig. 8

(a)

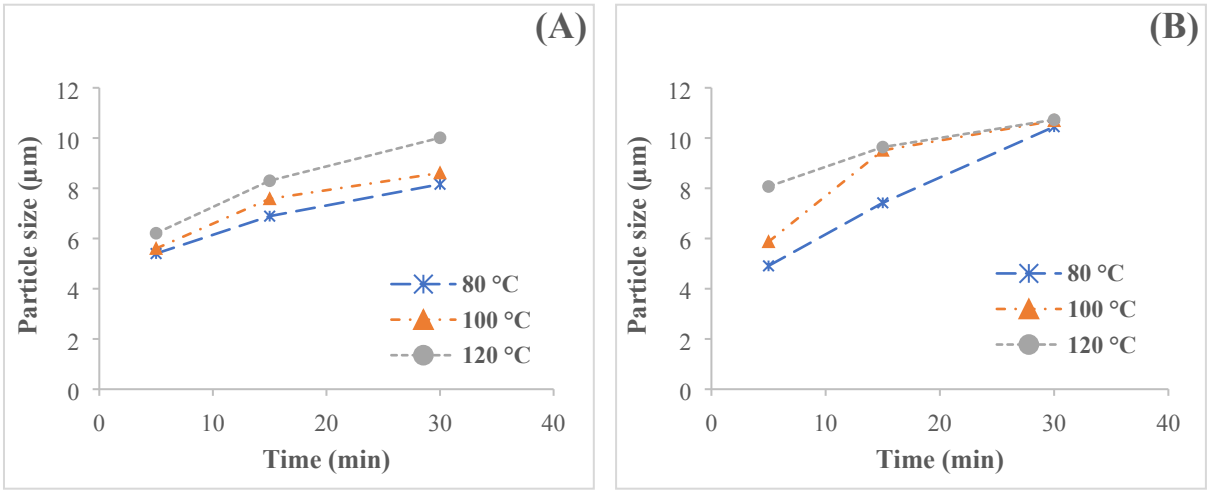
(A)
Particle size (µm)
Time (min)
80 °C
100 °C
120 °C
(B)
Particle size (µm)
Time (min)
80 °C
100 °C
120 °C

(b)

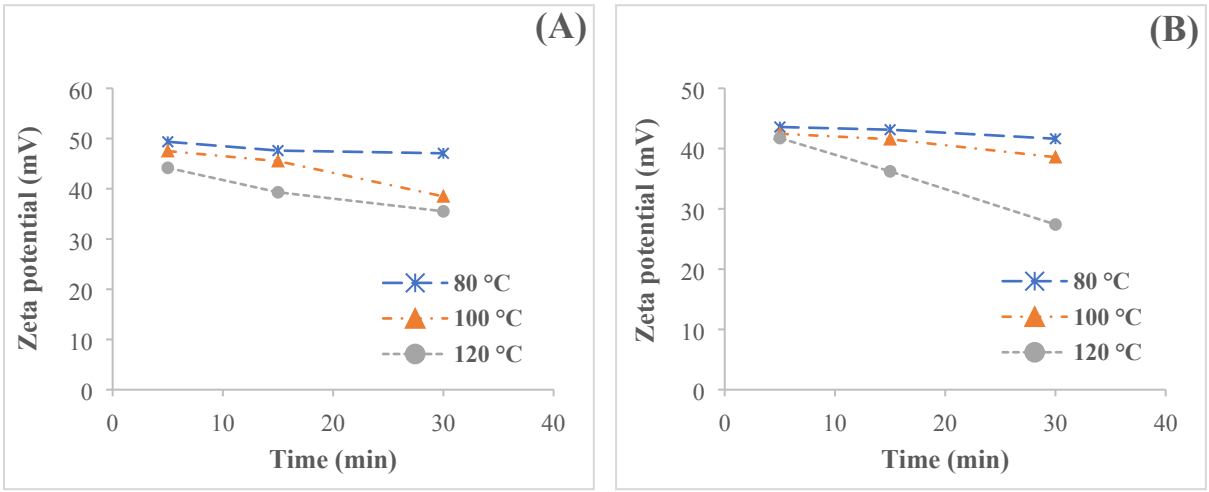
(A)
Zeta potential (mV)
Time (min)
80 °C
100 °C
120 °C
(B)
Zeta potential (mV)
Time (min)
80 °C
100 °C
120 °C

Fig. 9

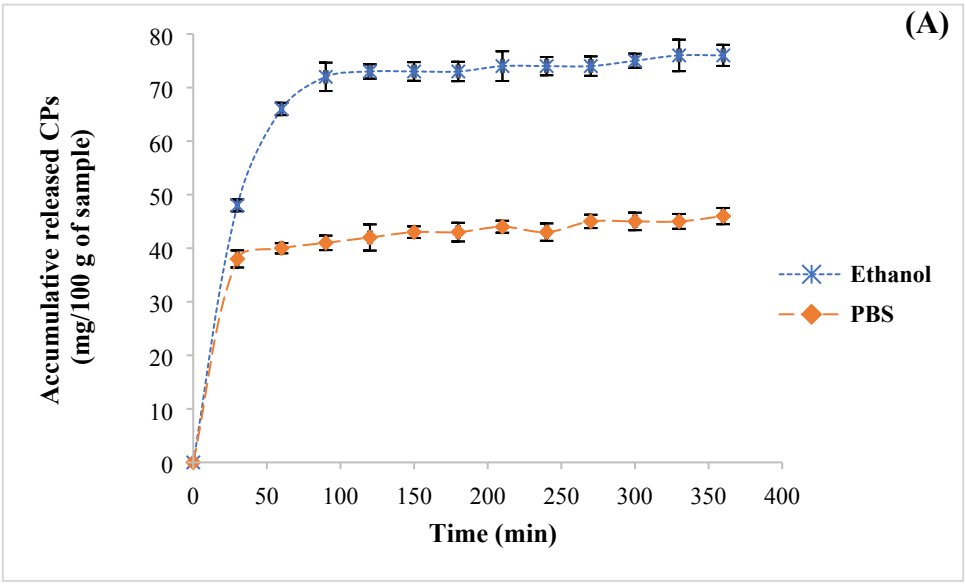
(A)
Accumulative released CPs (mg/100 g of sample)
80
70
60
50
40
30
20
10
0
0
50
100
150
200
250
300
350
400
Time (min)
Ethanol
PBS

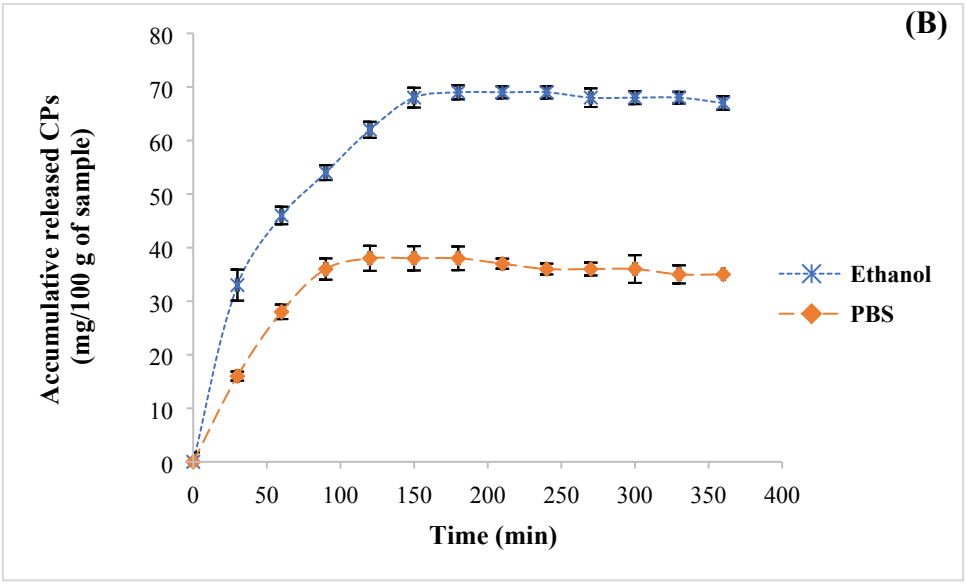
(B)
Accumulative released CPs (mg/100 g of sample)
80
70
60
50
40
30
20
10
0
0
50
100
150
200
250
300
350
400
Time (min)
Ethanol
PBS

Ionotropic Gelation

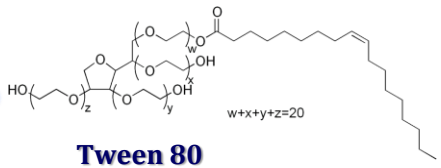

Tween 80

Emulsification

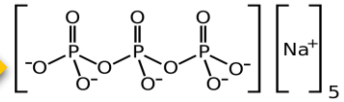

TPP added

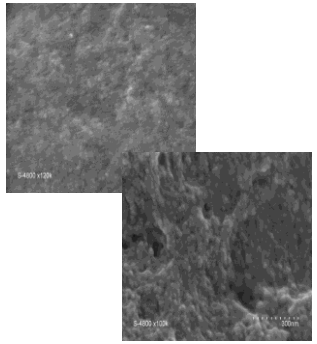

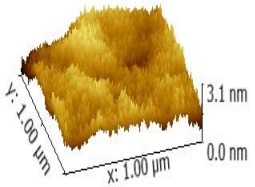

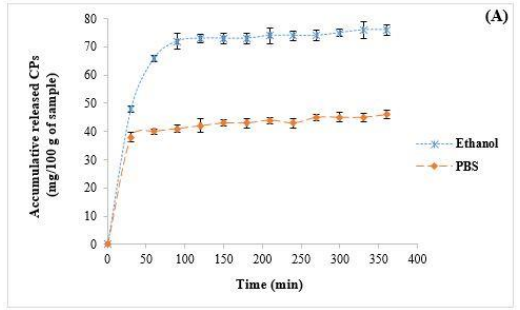

In vitro release

Chitosan BCC
AD = 8%
Mw = 115 000 g mol^{-1}

Carotenoproteins
CPs

Proteins Isolate
BCPI

pH 6.0
BCC to BCPI of 1/8

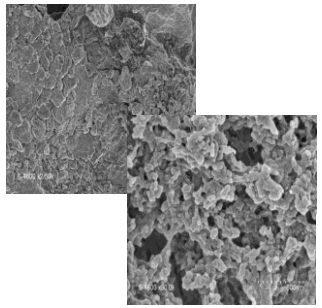

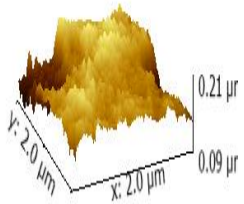

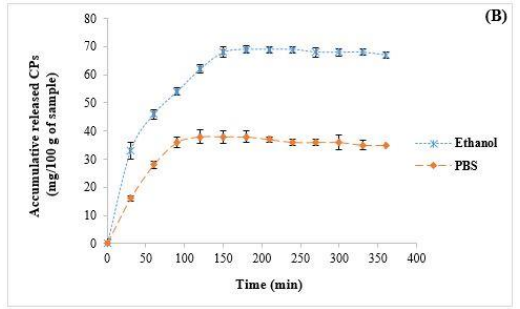

In vitro release

Complex Coacervation

Table 1: Particle size (µm), polydispersity index (%) and zeta potential (mV) of CS-based nanocapsules.

		Particle size (µm)	Polydispersity index (%)	Zeta potential (mV)
Ionotropic gelation	unloaded CS	7.26 ± 0.01^{aB}	42.90	51.43 ± 0.73^{aA}
	CPs-loaded CS	4.72 ± 0.06^{bB}	37.94	45.30 ± 1.38^{bA}
Complex coacervation	unloaded CS	9.76 ± 0.09^{aA}	62.37	49.42 ± 0.68^{aB}
	CPs-loaded CS	4.87 ± 0.01^{bA}	47.04	46.80 ± 0.24^{bB}

CPs: carotenoproteins; **CS:** blue crab chitosan.

* Results are the means of three determinations ± standard deviation.

(a-b) Different letters in the same column are significantly different for the same process, as determined by ANOVA test ($p < 0.05$).

(A-B) Different letters in the same column are significantly different between the ionotropic gelation and the coacervation complex approaches, as determined by ANOVA test ($p < 0.05$).

Table 2: Encapsulation efficiency (%) and loading charge (%) of CPs into CS-based nanocapsules.

	EE (%) *	LC (%) **
Ionotropic gelation	88.54	46.43
Complex coacervation	73.93	31.87

CPs: carotenoproteins extract; **CS:** blue crab chitosan; **EE:** encapsulation efficiency; **LC:** loading charge.

* The loading capacity (LC%) is defined as the quantity of loaded CPs per 100 g of nanoparticles.

** The encapsulation efficiency (EE%) corresponded to the amount of loaded CPs based on the initial CPs (in feed).